J. Fluid Mech. (2006), *vol.* 565, *pp.* 279–318.
doi:10.1017/S0022112006001698 Printed in the United Kingdom

Algebraic and exponential instability of inviscid swirling flow

By C. J. HEATON AND N. PEAKE

Department of Applied Mathematics and Theoretical Physics, University of Cambridge, Wilberforce Road, Cambridge CB3 0WA, UK

(Received 28 July 2005 and in revised form 24 March 2006)

In this paper we consider the spectrum and stability properties of small-amplitude waves in three-dimensional inviscid compressible swirling flow with non-zero mean vorticity, contained in an infinitely long annular circular cylinder. The mean flow has swirl and sheared axial components which are general functions of radius. We describe the form of the spectrum, in particular the three distinct types of disturbance: sonic (or acoustic) modes; nearly-convected modes; and the non-modal continuous spectrum. The phenomenon of accumulation of infinitely many eigenvalues of the nearly-convected type in the complex wavenumber-plane is classified carefully: we find two different regimes of accumulating neutral modes and one regime of accumulating instability modes, and analytic conditions for the occurrence of each type of behaviour are given. We also discuss the Green's function for the unsteady field, and in particular the contribution made by the continuous spectrum. We show that this contribution can grow algebraically downstream, and is responsible for a new type of convective instability. The algebraic growth rate of this instability is a complicated function of the mean flow parameters, and can be arbitrarily large as a function of radius in cases in which the local convected wavenumber has a local extremum. The algebraic instability we describe is additional to any conventional modal instability which may be present, and indeed we exhibit cases which are convectively stable to modes, but which nevertheless grow algebraically downstream.

1. Introduction

This paper considers the acoustics and stability of inviscid swirling flow. Acoustic problems with swirling flow have many potential applications, most obviously to aeroacoustics; however, the presence of vorticity in the mean flow complicates the usual acoustic problem. Golubev & Atassi (1998) termed the disturbances 'acoustic–vorticity waves', finding a combined spectrum containing two distinct families of modes, respectively analogous to the acoustic and vorticity waves found in irrotational flow. We consider these waves, discussing properties of the eigenvalue spectrum and also the waves' stability properties. In particular, a family of so-called nearly-convected modes often has an infinite accumulation of eigenvalues in the complex plane and we classify this, finding in some cases a family of instability modes. We then turn to the continuous spectrum of the acoustic–vorticity waves and find that it too can be responsible for instability, now with algebraic growth.

The stability of swirling inviscid flow has been considered by many previous authors, most notably by Rayleigh (1916). Rayleigh's famous stability criterion concerns axisymmetric perturbations to incompressible rotating fluid and many authors have

extended this in various directions. Pedley (1968, 1969) considered an asymptotic class of inviscid pipe flows, with superimposed rotations of approximately rigid-body type, and found unstable modes at large wavelength. Leibovich & Stewartson (1983), and a series of follow-up papers, used WKB theory to find unstable modes at asymptotically large azimuthal wavenumbers in a wide class of swirling flows. The family of unstable nearly-convected modes we identify is shown to correspond to the modes of Leibovich & Stewartson (1983), and among the conclusions drawn from our analysis is an extension of their results to finite azimuthal orders. The non-modal instability we identify and investigate in the latter part of this paper is due to the continuous spectrum of the linearized Euler equations, and is in addition to any modal growth that may or may not be present. As such, the stability results we present for this are complementary to most of the large literature on swirling flow stability. (Note that we reserve the word 'mode' for an analytic eigenfunction associated to a discrete eigenvalue. So-called 'singular modes' are non-modal in this terminology, and we will show that they require a quite different mathematical treatment.) Both Howard & Gupta (1962) and Lalas (1975) used energy arguments to derive sufficient stability criteria for incompressible and compressible swirling flows, respectively; these criteria guarantee stability to modal and non-modal disturbances alike and so can be compared to our results. Many authors have investigated the critical layer and associated continuous spectrum of two-dimensional shear flow, beginning with Rayleigh (1896); the first modern paper concerned primarily with the 'continuous spectrum' being that of Case (1960). Some classical results and asymptotic analysis of critical layers and viscous sublayers are given by Drazin & Reid (1981). The continuous spectrum of parallel shear flow has been found to lead to linear growth of the flow energy by Landahl (1980) and Hanifi & Henningson (1998). In the present work, we find richer behaviour due to the critical layer of a swirling flow, which appears to be a result of taking a fully three-dimensional flow. We work at a fixed real temporal frequency and consider spatial growth for most of our stability analysis because our original motivation is in aeroacoustics, where the frequency is given and the physically relevant problem is the spatial development. Direct comparison to the temporal stability problems cited can be made, however, and we do so at the end of the paper.

Recent investigations into acoustic–vorticity waves include those of Golubev & Atassi (1998), Tam & Auriault (1998) and Nijboer (2001). The possible existence of 'convected/singular modes', i.e. a continuous spectrum, in swirling flow has been disputed in the aeroacoustics literature, and this aspect is of particular interest to us here: we will show that such a spectrum does exist and present the first full and correct treatment of it. Golubev & Atassi (1998) considered the spectrum of acoustic–vorticity waves in several cases: they chose a uniform axial velocity and an azimuthal velocity of the form $(\Omega r + \Gamma/r)\boldsymbol{e}_\theta$, a mixture of solid-body rotation and free-vortex swirl. Solving the eigenvalue problem for the axial wavenumber k numerically, with a spectral approach, they report spectra with discrete pressure-dominated (or *sonic*) modes analogous to acoustic modes in irrotational flow. They also point out that their eigenvalue problem has a critical layer, corresponding to perfect convection of the unsteady disturbance, and leading to a forbidden interval of the real k-axis on which the eigenfunctions would be singular. At either end of this interval they see clustering of infinitely many discrete rotational (or *nearly-convected*) modes. These modes are difficult to resolve numerically, and Golubev & Atassi (1998) make an attempt to describe the asymptotic accumulation. Their asymptotic analysis is incomplete, however, and is also based on a thin-annulus approximation which cannot strictly be applied to the infinite tail of the accumulation. In this paper, we perform asymptotic

calculations which do not rely on the thin-annulus approximation, and which are applicable to a wider class of flows.

Tam & Auriault (1998) perform a similar analysis to Golubev & Atassi (1998) to look for the modes of the spectrum, which they do by defining a dispersion relation $D(k,\omega)$ and looking for the zeros of this function in the complex k-plane. Their method successfully finds the acoustic modes of the system, but fails near the convected wavenumbers: they assert that no purely convected disturbances exist because they find no zeros of $D(k,\omega)$ in the vicinity of pure convection. In fact convected disturbances do exist, but they are not of a straightforward modal type, and as such are not zeros of a dispersion relation. Further, an unstable mode is found by Tam & Auriault, which has crossed from $\mathrm{Im}(k)>0$ into $\mathrm{Im}(k)<0$ as the imaginary part of temporal frequency is reduced to zero in the standard Briggs–Bers way. This mode therefore leads to a convective instability in which the disturbance grows exponentially downstream. This is because Tam & Auriault's swirling mean flow has a uniform density, making it inherently unstable. One expects the density of a swirling compressible flow to increase with radius because of centrifugal forces, and indeed this is the case: compressible swirling flows have strong parallels to stratified shear flows in the presence of gravity (see Lalas 1975 for more details and further references). In fact, the radial variation of density in a swirling flow can be used to construct an analogue of the Brunt–Väisälä frequency N, as given by (2.20) below. For Tam & Auriault's mean flow, $N^2<0$ and the flow is unstable for this reason. In this paper, we consistently take a homentropic mean flow, i.e. $p\propto\rho^{\gamma}$ with γ the ratio of specific heats, and in this case $N^2=0$, so that 'stratification' is neither stabilizing nor destabilizing the flow and does not interfere with our investigation of acoustic–vorticity waves.

Finally, Nijboer (2001) made a numerical investigation of the spectra for several different cases of swirling flows of the type considered by Tam & Auriault (1998) and Golubev & Atassi (1998). The numerics of this investigation are well converged, and indeed the now familiar features of the spectrum are well observed. Nijboer makes several empirical observations based on his results, most notably concluding that there is a continuum of convected modes because every gridpoint appears to be a mode on that section of the real k-axis.

The remainder of this paper is set out as follows. In § 2 we give the governing equations, review the spectrum of acoustic–vorticity modes and argue that a continuous spectrum of convected modes does exist. In § 3 we describe the asymptotic accumulation in the complex plane of nearly-convected modes: §§ 3.1 and 3.2 describe two types of neutral mode and § 3.3 describes a set of unstable modes. Numerical examples of the different accumulation rates are presented in § 3.4. In § 4 we consider the Green's function for disturbances to a swirling flow and find a new convective algebraic instability due to the continuous spectrum. In § 4.3 we give some numerical calculations which demonstrate this instability. In § 5 we discuss a high-frequency asymptotic limit, in order to draw correspondence between our results and some existing results in the aeroacoustics literature. In § 6 we discuss the results on flow stability of the present paper in relation to the stability criteria for inviscid flow in the existing literature. Some final conclusions are drawn in § 7.

2. The spectrum of acoustic–vorticity waves

2.1. *The governing equations*

The geometry we consider is an infinite cylindrical annulus, $h\leqslant r\leqslant 1$ in cylindrical polar coordinates (r,θ,x), with hard impermeable walls at $r=h,1$. Throughout, we

non-dimensionalize lengths by the outer radius of the duct, densities by the mean density at $r = 1$ and velocities by the mean sound speed at $r = 1$. We neglect dissipation and consider compressible inviscid flow with total velocity of the form

$$\boldsymbol{U}_{tot}(x, r, \theta, t) = \boldsymbol{U}_0(r) + \boldsymbol{u}'(x, r, \theta, t), \tag{2.1}$$

being a steady mean flow plus a small unsteady perturbation. We consider a three-dimensional axisymmetric subsonic mean flow of the form

$$\boldsymbol{U}_0 = U(r)\boldsymbol{e}_x + W(r)\boldsymbol{e}_\theta. \tag{2.2}$$

The mean flow and the perturbation are assumed homentropic. The presence of mean vorticity prohibits the use of a simple scalar acoustic potential to describe the perturbations, and instead we use a decomposition of the unsteady velocity due to Goldstein (1978),

$$\boldsymbol{u}' = \boldsymbol{u} + \nabla\phi. \tag{2.3}$$

The unsteady potential ϕ is chosen so that the unsteady pressure, p', is given solely in terms of ϕ, i.e.

$$p' = -\rho_0 \frac{\mathrm{D}_0\phi}{\mathrm{D}t}, \tag{2.4}$$

where ρ_0 is the local mean density and $\mathrm{D}_0/\mathrm{D}t$ is the mean-flow Lagrangian derivative. This gauge condition ensures that ϕ is the correct analogue of the acoustic potential of irrotational mean flow. The linearized equations of conservation of momentum and mass then become

$$\frac{\mathrm{D}_0\boldsymbol{u}}{\mathrm{D}t} + \boldsymbol{u}\cdot\nabla\boldsymbol{U}_0 = -\boldsymbol{\xi}_0 \wedge \nabla\phi, \tag{2.5}$$

$$\frac{\mathrm{D}_0}{\mathrm{D}t}\left(\frac{1}{c_0^2}\frac{\mathrm{D}_0\phi}{\mathrm{D}t}\right) - \frac{1}{\rho_0}\nabla\cdot(\rho_0\nabla\phi) = \frac{1}{\rho_0}\nabla\cdot(\rho_0\boldsymbol{u}), \tag{2.6}$$

respectively, where c_0 is the local mean flow sound speed and $\boldsymbol{\xi}_0 = r^{-1}(rW)'\boldsymbol{e}_x - U'\boldsymbol{e}_\theta$ is the vorticity of the mean flow. It is clear that the presence of mean vorticity, $\boldsymbol{\xi}_0 \neq 0$, couples the two portions of the unsteady velocity together. In particular, the unsteady vorticity is coupled to the unsteady pressure, and hence the waves sustained by this flow are termed 'acoustic–vorticity' waves. The boundary conditions for (2.5) and (2.6) are zero normal (i.e. radial) flow on the duct walls,

$$(\boldsymbol{u} + \nabla\phi)\cdot\boldsymbol{e}_r = 0. \tag{2.7}$$

We take Fourier transforms in x and time t, and without loss of generality we also decompose the disturbance into a Fourier series in θ and consider each term separately. Hence all unsteady perturbations are proportional to $\mathrm{e}^{-\mathrm{i}\omega t + \mathrm{i}m\theta + \mathrm{i}kx}$ for $m \in \mathbb{Z}$. We shall seek causal solutions to the governing equations, so implicit in these statements is the notion that we will adhere to the Briggs–Bers technique (Briggs 1964; Bers 1983) for deforming the relevant Fourier inversion contours. This technicality is crucially important when it comes to determining the stability of the flow, and it will also be key to identifying and treating the convected continuous spectrum. From (2.4) we therefore have

$$p' = -\mathrm{i}\rho_0\Lambda(k, r)\phi, \tag{2.8}$$

where

$$\Lambda(k, r) = Uk - \omega + mW/r \equiv U(k - k_c) \tag{2.9}$$

corresponds to the operator $\mathrm{D}_0/\mathrm{D}t$, and

$$k_c(r) = (\omega - mW(r)/r)/U(r) \tag{2.10}$$

is the axial wavenumber corresponding to pure convection of the unsteady perturbation at radius r. We write the axial Fourier transforms of the unsteady field as

$$\phi = \phi(r)\mathrm{e}^{\mathrm{i}kx+\mathrm{i}m\theta-\mathrm{i}\omega t}, \quad \boldsymbol{u} = (\mathscr{R}(r), T(r), X(r))\mathrm{e}^{\mathrm{i}kx+\mathrm{i}m\theta-\mathrm{i}\omega t}, \tag{2.11}$$

mirroring the notation used by Golubev & Atassi (1998). The three components of the unsteady momentum equation (2.5) give

$$\mathscr{R}D = \Lambda G\phi + \frac{2W(Wr)'}{r^2}\phi' \tag{2.12}$$

$$TD = \frac{\mathrm{i}(Wr)'}{r}[G\phi + \Lambda\phi'] \tag{2.13}$$

$$XD = \mathrm{i}U'[G\phi + \Lambda\phi'], \tag{2.14}$$

where prime denotes differentiation with respect to r and we define, for ease of notation,

$$G = U'k + m(Wr)'/r^2, \tag{2.15}$$

$$D = \Lambda^2 - 2W(Wr)'/r^2. \tag{2.16}$$

The equation of mass conservation (2.6) gives

$$\phi'' + \phi'\left(\frac{1}{r} + \frac{\rho_0'}{\rho_0}\right) + \phi\left(\frac{\Lambda^2}{c_0^2} - \frac{m^2}{r^2} - k^2\right) + \mathscr{R}' + \mathscr{R}\left(\frac{1}{r} + \frac{\rho_0'}{\rho_0}\right) + \frac{\mathrm{i}mT}{r} + \mathrm{i}kX = 0, \tag{2.17}$$

which is the same as equation (13) of Golubev & Atassi (1998). In the present study, the mean flow and unsteady perturbations are assumed homentropic (the implications of which will be fully discussed in § 6 below), so that

$$c_0^2 = 1 + (\gamma - 1)\int_1^r \frac{W(t)^2}{t}\,\mathrm{d}t, \tag{2.18}$$

where γ is the constant ratio of specific heats, and also

$$r\rho_0'/\rho_0 = W^2/c_0^2. \tag{2.19}$$

The homentropic assumption implies that the swirling flow analogue of the Brunt–Väisälä frequency $N^2 = 0$, where N^2 is given by (see equation (2.20) of Lalas 1975)

$$N^2 = \left(\rho_0' - \frac{p_0'}{c_o^2}\right)\frac{W^2}{r\rho_0}. \tag{2.20}$$

Therefore we are concentrating here on the hydrodynamic stability alone. Our results should be suitably modified by the stabilizing (or destabilizing) effect of a background density 'stratification' if present in a real problem. We can combine equations (2.12)–(2.14) and (2.17) to give the mode-shape equation, a second-order ordinary differential equation for the unsteady potential,

$$\frac{1}{r\rho_0}\frac{\mathrm{d}}{\mathrm{d}r}\left(\frac{r\rho_0\Lambda(G\phi + \Lambda\phi')}{D}\right) - \frac{G}{D}(G\phi + \Lambda\phi') + \phi\left(\frac{\Lambda^2}{c_0^2} - \frac{m^2}{r^2} - k^2\right) = 0. \tag{2.21}$$

2.2. *The discrete modes and the continuous spectrum*

Inspection of (2.21) shows that it has singularities when $D = 0$, and when $\Lambda = 0$ (so that the coefficient of the highest derivative vanishes). In fact $D = 0$ is a removable

singularity, because (2.12)–(2.14) show that, for a smooth mean flow, $D=0 \Rightarrow G\phi + \Lambda\phi' = 0$. This point plays no further part in our discussion of the flow stability, but must be understood for effective numerical calculation, and for this reason we choose to integrate (2.21) in vector form by writing

$$\begin{pmatrix} z_1 \\ z_2 \end{pmatrix} = \begin{pmatrix} r\rho_0\phi \\ r\rho_0\Lambda(G\phi + \Lambda\phi')/D \end{pmatrix}, \tag{2.22}$$

so that (2.21) becomes

$$\frac{\mathrm{d}}{\mathrm{d}r}\begin{pmatrix} z_1 \\ z_2 \end{pmatrix} = \begin{pmatrix} -G/\Lambda + \left(1 + W^2/c_0^2\right)/r & D/\Lambda^2 \\ -\Lambda^2/c_0^2 + m^2/r^2 + k^2 & G/\Lambda \end{pmatrix}\begin{pmatrix} z_1 \\ z_2 \end{pmatrix}. \tag{2.23}$$

It is now clear that $\Lambda = 0$ is the only genuine singularity of (2.21) and it is this singularity, which corresponds to the disturbance being purely convected, that is termed the *critical layer* of the equation.

The spatial eigenvalue problem for the discrete modes of the system corresponds to determining those k for which there is a non-trivial solution of (2.21) subject to the impermeability boundary conditions (2.7), which now become

$$\mathscr{R} + \phi' = \Lambda(G\phi + \Lambda\phi')/D = 0, \quad r = h, 1. \tag{2.24}$$

These eigenvalues and eigenfunctions give the modes of the system, and correspond to zeros of the dispersion relation. Note that the eigenvalue problem defined by (2.21) and (2.24) is not of Sturm–Liouville form, and hence the modes are not normal, and do not form a complete basis.

We now define the set of points in the complex k-plane such that a critical layer appears in the duct, $h \leqslant r \leqslant 1$, as

$$C_k = \{k_c(r) : h \leqslant r \leqslant 1\}. \tag{2.25}$$

For any $k \in C_k$ there exists at least one physical radius r_c (by *physical* we mean that $r_c \in \mathbb{R}$ and $h \leqslant r_c \leqslant 1$) at which $\Lambda(r_c, k) = 0$ and this is usually a regular singular point (RSP) of the differential equation (2.21). Note that if $k_c(r)$ is not a monotonic function of r, then there may be multiple critical layers in the duct for a given wavenumber k. More generally, for $k \notin C_k$ there still exist solutions r_c of $\Lambda(r_c, k) = 0$, which are RSPs of (2.21) and which are termed critical radii, however they are not physical radii in the sense described above (typically the r_c are complex for $k \notin C_k$). Close to a RSP, solutions of the differential equation can be written in the form of a Frobenius expansion

$$\phi(r) = (r - r_c)^\sigma \sum_{n=0}^{\infty} a_n (r - r_c)^n, \tag{2.26}$$

where $a_0 \neq 0$ and the exponents σ satisfy the indicial equation. If

$$\left.\frac{\partial}{\partial r}\Lambda(k, r)\right|_{r=r_c, k=k_c(r)} \neq 0, \tag{2.27}$$

then $r = r_c$ is indeed an RSP of (2.21) when $k = k_c(r)$, and the indices are given by

$$\sigma = -\tfrac{1}{2} \pm \sqrt{\tfrac{1}{4} - A(r_c)}, \tag{2.28}$$

where

$$A(r) = \frac{2Wk_c(k_c(Wr)' - mU')}{r^2(m(W/r)' + U'k_c)^2}. \tag{2.29}$$

Equations (2.28) and (2.29) reduce to the exponents found in Golubev & Atassi (1998) and Nijboer (2001) for the mean flows considered in those papers. Note that the denominator in the definition of A, (2.29), being zero corresponds to condition (2.27) failing. In this case, $r = r_c$ is not an RSP but is a stronger singularity of the differential equation, and this case will be treated separately below. From (2.28), we see that the solution ϕ must blow up at the critical layer $r = r_c$, and that if $A > 1/4$ then the exponents are complex. In this latter case, ϕ also oscillates more and more rapidly as $r \to r_c$,

$$\phi \sim \alpha(r - r_c)^{-1/2} \sin(\sqrt{A(r_c) - 1/4}\log(r - r_c) + \beta)$$

as $r \to r_c$, with some constants α and β. In any event, the general solution of (2.21) is singular at the critical radius, and this is not permissible.

More precisely, since we wish, in principle, to invert the axial Fourier transform, using an integration contour defined by the Briggs–Bers procedure, we note that $\phi(k, r)$ is not holomorphic in k for $k \in C_k$, and so we must cut the complex k-plane along the section of the real axis given by C_k. This then implies the existence of convected disturbances, of a non-modal type: the final step of any calculation must be the inversion of the axial Fourier transform, using a suitably deformed inversion contour to ensure causality (for example, see the swirling flow scattering problems considered by Heaton & Peake (2005) or the Green's function calculations in § 4 below). Poles in the inversion integrand will give modal contributions to the solution, whereas closing the inversion contour in the appropriate half-plane and having to wrap the contour around the branch cut, C_k, will inevitably lead to non-modal contributions to the solution. This conclusion agrees with the assertions by Golubev & Atassi (1998) and Nijboer (2001) that there exist 'convected modes', whereas the conclusion of Tam & Auriault (1998, p. 18) that such modes are spurious numerical results is incorrect. The singular nature of the solution at the critical layer makes numerical computation of ϕ and the dispersion relation difficult close to convection, which is why the previous numerical investigations of acoustic–vorticity waves have failed to agree on the existence of convected disturbances. The crucial effect of the continuous spectrum will be demonstrated explicitly in § 4.

The overall picture in the complex k-plane can now be described in full, and a schematic picture is given in figure 1. There is a family of modes variously termed 'sonic', 'pressure-dominated', or 'acoustic', which are the analogues of the acoustic waves in irrotational flow. These modes are sustained by compressibility and have little vortical velocity. The branch cut C_k lies on the real k-axis, and defines a continuous spectrum which contributes non-modal disturbances as outlined above. Finally, there may be a second family of modes termed 'nearly-convected' or 'rotational', close to C_k in the complex k-plane. There can be an infinite number of nearly-convected modes clustering near to the ends of C_k. Together, the nearly-convected modes and the continuum of convected wavenumbers C_k are the analogues of the pressure-less vorticity waves in irrotational flow. This part of the spectrum generally has smaller pressure than the sonic modes because of (2.8), but nevertheless the discrete nearly-convected modes were shown to contribute, substantially in some circumstances, to the unsteady pressure (and hence the noise) by Heaton & Peake (2005) in some physically motivated problems, so we anticipate that the contribution from C_k may also be important. Another possibility, which we will see in § 3.3, is that an infinite accumulation of convectively unstable modes can exist in place of the infinite family of nearly-convected neutral modes shown in figure 1.

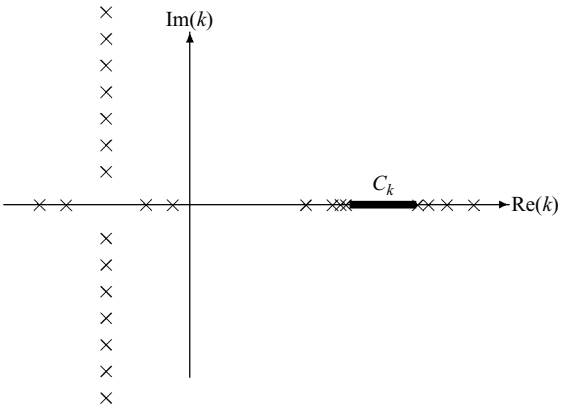

FIGURE 1. A schematic picture of the complex k-plane, for a typical swirling flow. The wavenumbers of the discrete modes are shown by $\times$, the set C_k of forbidden values on the real axis along which the complex plane is cut is shown by a thick line.

3. Results on the clustering of nearly-convected modes

This section aims to give a self-contained discussion of the phenomenon of clustering of nearly-convected modes at the ends of the cut C_k. This appears to be a generic feature of swirling flow, having been observed in the calculations of Golubev & Atassi (1998), Nijboer (2001) and Heaton & Peake (2005). In this section, our aim is to identify when clustering occurs and when it does not, and when it does to derive the asymptotic accumulation rate of the modal eigenvalues. This latter calculation is an important technicality because one needs to know the convergence properties of any infinite sum of such modes, especially if the ultimate aim is to evaluate the sum on a computer. This issue was encountered by Heaton & Peake (2005), where the infinite sums of nearly-convected modes in a problem with the special case of rigid-body swirling flow were shown to converge and then evaluated numerically. The general trend is that nearly-convected modes clustering towards C_k have highly-oscillatory mode shapes which are expensive to calculate, so knowledge of when to truncate an infinite sum of clustering modes is, in fact, computationally very important.

Before beginning our calculation, we note that Nijboer (2001) gives a heuristic argument for a 'cluster condition', which in our notation requires $A(r) > 1/4$ at $r = h$ or $r = 1$, with $A(r)$ given by (2.29). We will prove that this result is indeed correct in some cases (§ 3.1), but we also encounter cases where it is not appropriate (§§ 3.2 and 3.3) and for these we derive the alternative condition. Also, Golubev & Atassi (1998) have considered the asymptotic accumulation rate of the nearly-convected modes. Again, the answers they give are correct in the cases they consider (§ 3.1), but there is a wide class of cases for which their results are not appropriate (§ 3.2 and § 3.3). We note also that Golubev & Atassi (1998, p. 218) assume that, if ϵ is the distance between the nearly-convected mode's eigenvalue wavenumber and the end of the cut C_k in the k-plane, then

$$1 - h = O(\epsilon) \ll 1. \tag{3.1}$$

This 'narrow annulus approximation' cannot in general be applied to the infinite tail of the accumulating sequence, because the asymptotic accumulation of eigenvalues for a particular set of flow parameters involves the $\epsilon \to 0$ limit of the eigenvalues for a fixed duct. No matter how narrow the annulus may be, once the geometry is chosen, (3.1) must fail for the modes with sufficiently small ϵ, and so the asymptotic accumulation

rate of the modes cannot be properly inferred from such an argument. We will show that the narrow annulus assumption (3.1) would imply an incorrect accumulation rate for the cases in §§ 3.2 and 3.3, although it does give the correct answer in the case considered by Golubev & Atassi (1998) and in § 3.1. After presenting the results for the possible asymptotic accumulation rates we then give in § 3.4 the first quantitative comparison to appear in the literature between predicted accumulation rates and numerically calculated spectra.

3.1. *The simplest case–$k_c(r)$ monotonic in r*

The first case to consider is that in which the relevant end of the cut C_k is given by one of $k_c(h)$ or $k_c(1)$, in other words the global maximum/minimum of $k_c(r)$ for $r \in [h, 1]$ is at an endpoint of the interval. Without loss of generality, we will take the smallest wavenumber on the cut to be $k_c(h)$ and hence consider modes approaching this wavenumber from below. Also we assume condition (2.27) holds at $r = h$, which is equivalent to $k_c'(h) \neq 0$, in order to consider the simplest generic case. In this case, the 'cluster condition' suggested by Nijboer (2001) and the accumulation rate of Golubev & Atassi (1998) will be shown to be correct.

Let us assume the eigenvalue wavenumber of a nearly-convected mode very close to the end of the cut is

$$k = k_c(h) - \epsilon, \tag{3.2}$$

where $0 < \epsilon \ll 1$. In this case, the critical layer is located at

$$r_c = h - \frac{\epsilon}{k_c'(h)} + O(\epsilon^2), \tag{3.3}$$

and by the assumptions above we know that $r_c < h$. Thus, as anticipated in the discussion following (2.25), since $k \notin C_k$, the RSP r_c is not located at a physical radius in the duct. Our asymptotic analysis now begins with the observation that $\Lambda(k, r) = O(\epsilon)$ when $r - h = O(\epsilon)$, and $\Lambda(k, r) = O(1)$ otherwise in the duct.

Consider integrating equation (2.21) from $r = h$, where condition (2.24) is applied (together with, for definiteness, $\phi = 1$ on $r = h$) towards $r = 1$, where applying condition (2.24) again will give an equation for ϵ, so determining the eigenvalue wavenumber k for small ϵ. This problem has two asymptotic regions of interest; an inner region with inner coordinate $R = (r - r_c)/\epsilon$, which has $R = O(1)$ near the critical layer, and an outer region comprising the rest of the duct. For $R = O(1)$, the leading-order solution of (2.21) is of the form

$$\phi \propto R^{-1/2} \sin(\mathrm{Im}(\sigma) \log R + \psi), \tag{3.4}$$

where σ is the complex exponent given by (2.28) with $r = h$, and $A(h) > 1/4$ is assumed. In order to apply the boundary conditions (2.24) it is convenient to consider $\chi(r) = G\phi + \Lambda\phi'$, for which the boundary conditions become $\chi(h) = \chi(1) = 0$. It is easily shown that χ has the same form (3.4) as ϕ in the inner region. We now have to extend this result beyond the inner region in which $R = O(1)$ in order to make further progress. This is done by asymptotic matching onto a solution to (2.21) valid in the rest of the duct, using Van Dyke's matching procedure (see for example Bender & Orszag (1978) for details). In practice, this would be a numerical undertaking because the solutions to (2.21) in the outer asymptotic region, $r - h = O(1)$, cannot be written down analytically. Nevertheless, a matching outer solution can easily be shown to exist and we can find the leading-order accumulation we seek by a simple analytical argument: we form a multiplicative composite of the two solutions, which is uniformly

valid in $h \leqslant r \leqslant 1$ as $\epsilon \to 0$. The composite is of the form

$$\chi \sim \mathscr{F}(r) R^{-1/2} \sin\left(\mathrm{Im}(\sigma) \log R + \psi\right), \tag{3.5}$$

where $\mathscr{F}(r)$ is some $O(1)$ function of radius, determinable numerically. Now applying the boundary conditions $\chi(h) = \chi(1) = 0$ gives

$$\mathrm{Im}(\sigma) \log\left(\frac{1 - r_c}{\epsilon}\right) + \psi = n_1 \pi, \quad \mathrm{Im}(\sigma) \log\left(\frac{h - r_c}{\epsilon}\right) + \psi = n_2 \pi \tag{3.6}$$

for integral n_1, n_2. Subtracting to eliminate ψ and rearranging we obtain at leading order

$$\mathrm{Im}(\sigma) \log(\epsilon^{-1}) \sim n\pi, \tag{3.7}$$

for $\epsilon \ll 1$ and $n \in \mathbb{Z}$. Therefore, for small ϵ,

$$\epsilon \propto \exp\left(\frac{-\pi n}{\mathrm{Im}(\sigma)}\right), \tag{3.8}$$

where n can be thought of as labelling the infinite sequence of nearly-convected modes, and the constant of proportionality is determined at the next order by the $O(1)$ terms in (3.7) which we have not calculated. This gives the asymptotic rate of accumulation for the modes, and will be verified numerically in § 3.4. We note also that when $A(h) < 1/4$ the exponent σ at the critical layer is real and the inner solution is no longer oscillatory as (3.4) was above, and hence a similar argument would yield that there is no infinity of solutions satisfying the boundary conditions as $\epsilon \to 0$. So, when $A(h) < 1/4$ there is no accumulation of modes at this end of the continuous spectrum.

A final observation to make is of the role played by the outer solution here: it plays a subordinate role in the final application of the boundary conditions to determine ϵ. The important effect is the oscillatory dependence of the inner solution on ϵ as it appears in the composite solution (3.5). The everywhere $O(1)$ outer solution merely transmits the sensitive behaviour of the inner solution to the boundaries, where we then apply the boundary conditions. This will be true also in the more complicated scenarios below.

3.2. *Clustering of stable modes when $k_c(r)$ is not monotonic*

Now we turn to the case when the assumptions at the beginning of § 3.1 fail, and take $k_c'(r) = 0$ at the end of the cut, so that

$$m(W/r)' + U'k = 0 \quad \text{at } r = r_c \tag{3.9}$$

in equation (2.29). This at first seems to be a very special case, although note that a rigid-body swirl with uniform axial flow belongs to this class of problems, as (3.9) holds for all r. This case is much more generic, however, because $k_c(r)$ need not be monotonic, and hence the largest or smallest wavenumber in C_k may very well be convected at some intermediate radius within the duct at which $k_c' = 0$. The clustering is then determined by the mean flow properties at this radius, not $r = h$ or $r = 1$. This observation identifies a large new class of problems for which the analysis of the previous section is inappropriate, and so we present the alternative results here.

Suppose that the maximum of $k_c(r)$ for $h \leqslant r \leqslant 1$ is at $r = d \in (h, 1)$, an internal radius of the duct, as depicted in figure 2 (an internal minimum can be treated in the same way). Note that in figure 2, and generally in the cases to which this discussion applies, there are multiple critical layers for some wavenumbers (two for

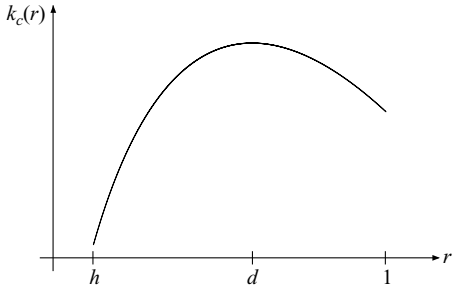

FIGURE 2. A schematic picture of $k_c(r)$, in a case for which the clustering of modes near to the maximum of C_k requires the analysis of § 3.2.

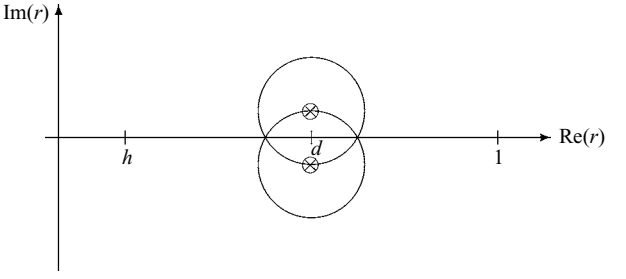

FIGURE 3. A schematic picture of the regular singular points (i.e. the critical layers), shown by ⊗, when $0 < \epsilon \ll 1$ in (3.10), together with corresponding circles of convergence.

$k_c(1) \leqslant k < k_c(d)$ in figure 2). In § 3.1, the end of the cut C_k just corresponded to the critical layer moving outside of the duct, whereas here we see that two critical layers merge as $k \nearrow k_c(d)$, and then both disappear (into the complex r-plane). We consider the possible clustering of nearly-convected modes to the right of C_k with wavenumber

$$k = k_c(d) + \epsilon, \tag{3.10}$$

where $0 < \epsilon \ll 1$. In this case, the leading-order change to the position of the critical layers is

$$r_c = d \pm \mathrm{i}\sqrt{\frac{-2\epsilon}{k_c''(d)}}, \tag{3.11}$$

assuming $k_c''(d) \neq 0$. Hence, rather than integrating (2.21) towards, but stopping just short of, a critical layer as in § 3.1, here we integrate from $r = h$ to 1 between these two RSPs, which are located just above and just below the real axis, as shown in figure 3. When $\epsilon = 0$, the two RSPs coincide on the real r-axis, and the differential equation (2.21) has an essential singularity.

The asymptotic nature of the solution to (2.21) is a little delicate. We shall see that there are three radial length scales of interest: the outer region, $r - d = O(1)$, and the inner region, $r - d = O(\epsilon)$, discussed in the simpler problem of § 3.1, and also an intermediate region for which $r - d = O(\epsilon^{1/2})$.

Consider first the inner region, for which $r - d = O(\epsilon)$. Since $\epsilon > 0$, (2.21) has two regular singular points near to which a Frobenius series solution can be found. Such a series solution has a finite radius of convergence, which is the distance in the complex plane to the next nearest singularity of the equation. This is shown in figure 3, and hence (3.11) implies that the Frobenius solution is valid on the real r-axis for

$$\text{For } r<d\text{: } \begin{cases} f_1(r) & \text{s.t.} \quad f_1(r)\sim (r-d)^{-1}\cos(\Theta) \\ f_2(r) & \text{s.t.} \quad f_2(r)\sim (r-d)^{-1}\sin(\Theta) \end{cases} \quad \text{as } r \nearrow d.$$

$$\text{For } r>d\text{: } \begin{cases} g_1(r) & \text{s.t.} \quad g_1(r)\sim (r-d)^{-1}\cos(\Theta) \\ g_2(r) & \text{s.t.} \quad g_2(r)\sim (r-d)^{-1}\sin(\Theta) \end{cases} \quad \text{as } r \searrow d.$$

TABLE 1. The outer region solutions for § 3.2. Away from $r=d$ they are smooth and $O(1)$, but only calculable numerically. The phase Θ is defined by (3.13).

$(r-d)/\epsilon^{1/2} < \sqrt{-6/k_c''(d)}$. The inner region is governed by this Frobenius solution– the exponents σ are found to be $O(\epsilon^{-1/2})$, and are real if $G^2 + D(m^2/d^2 + k^2) < 0$, a condition which reduces after a little algebra to

$$\frac{2Wk}{r^2}(k(Wr)' - mU') > 0, \tag{3.12}$$

evaluated at $r=d$, $k=k_c(d)$. Varying r along the real line in the inner region equates to a change of the complex phase (not amplitude) of $r-r_c$, as can be seen from figure 3. Hence the inner region Frobenius solution $(r-r_c)^\sigma$, which has exponents σ that are $O(\epsilon^{-1/2})$ large and real, has very oscillatory radial dependence. The outer solution will transmit this oscillatory behaviour to the boundaries so we can expect there to be many nearly-convected modes. Thus, we quickly see why nearly-convected modes will be present; however, the intermediate region and outer regions alone will turn out to be the distinguished limits in the calculation which follows.

Next we consider the outer region, away from the singularity, in which $r-d=O(1)$. The leading-order expression is found by setting $\epsilon=0$ which causes Λ to have a double zero (precisely: $\Lambda \sim U(d)k_c''(d)(r-d)^2/2$ as $r\to d$), so that the regular singular points appear coincident and the problem has an essential singularity at $r=d$. Nevertheless a solution can be found, in practice numerically, which is analytic away from $r=d$, and which we will attempt to match with the intermediate region below. As before, the outer solution plays a subordinate role in determining the asymptotic accumulation rate, and need not actually be calculated for the purposes of this argument. The behaviour near to the essential singularity at $r \simeq d$ is obtained by standard methods, see for example Bender & Orszag (1978). The dominant behaviour is rapid oscillation, as anticipated, with a phase given by

$$\Theta \equiv \frac{2\alpha}{(r-d)k_c''(d)}, \tag{3.13}$$

where α is defined in (3.16) below. We formally define two linearly independent outer region solutions for $r<d$ and $r>d$ in table 1. The solution in the outer region is just a linear combination of $f_{1,2}$ for $r<d$, or $g_{1,2}$ for $r>d$. One way to view the matching that follows is that it provides a connection formula between the coefficients of $f_{1,2}$ and $g_{1,2}$ in the two outer regions.

We define the intermediate asymptotic region such that the coordinate $\bar{R}$ is given by

$$\bar{R} = (r-d)/|\epsilon|^{1/2}. \tag{3.14}$$

The leading-order equation in the intermediate region (using the assumption that ϵ is real and positive) is

$$\frac{\mathrm{d}^2\Psi}{\mathrm{d}\bar{R}^2} = \frac{-1}{\epsilon(1-k_c''\bar{R}^2/2)^2}\left[\frac{2Wk_c(k_c(Wr)'-mU')}{r^2U^2}\right]\Psi + O(\epsilon^{-1/2}), \tag{3.15}$$

where we define $\Psi \equiv (1-R^2k_c''/2)\phi$ and all quantities U, W and k_c are evaluated at $r=d$. Provided (3.12) holds, we can write (3.15) as

$$\frac{\mathrm{d}^2\Psi}{\mathrm{d}\bar{R}^2} = \frac{-\alpha^2\Psi}{\epsilon(1-k_c''\bar{R}^2/2)^2}, \quad \alpha^2 = \left|\frac{2Wk_c(k_c(Wr)'-mU')}{r^2U^2}\right|. \tag{3.16}$$

Equation (3.16) can be solved analytically to give the two linearly independent solutions

$$\phi = \left(1-\frac{k_c''\bar{R}^2}{2}\right)^{-1/2}\exp\left\{\pm\mathrm{i}\sqrt{1-\frac{2\alpha^2}{k_c''\epsilon}}\tan^{-1}\left(\bar{R}\sqrt{\frac{-k_c''}{2}}\right)\right\}. \tag{3.17}$$

It is easily seen by taking the $\bar{R}$ derivative of the phase in (3.17), or indeed directly by inspection of (3.16), that the fastest radial oscillations occur when $\bar{R}=0$. The fastest oscillations are hence in the inner region, and have a length scale of $O(\epsilon)$, i.e. the length scale of the inner region. However, it is the intermediate region which provides the solution (3.17) which is suitable for matching with the outer solution, and this is the essential difference to the easier case of § 3.1.

It now remains to match the outer and intermediate regions. It can be seen by inspection of (3.17) in the limit $\bar{R}\to\pm\infty$ that the intermediate solution functionally matches the $r\to d$ limit of the outer solution given in table 1. It is convenient to phrase the matching at either end of the intermediate region in terms of providing a connection formula between the two outer regions, i.e. between the coefficients of the four functions defined in table 1. This viewpoint of the matching will be especially helpful when we extend the method to a more complicated scenario in § 3.3. Suppose that the outer region solutions which satisfy the boundary condition (2.24) at $r=h$, 1, respectively, are given by

$$\left.\begin{aligned}\phi &\propto f_1(r)+qf_2(r), \quad r<d,\\ \phi &\propto g_1(r)+Qg_2(r), \quad r>d.\end{aligned}\right\} \tag{3.18}$$

The real constants q, Q are $O(1)$ and could be determined numerically, though that will not be necessary here. Matching as $\bar{R}\to-\infty$ yields coefficients for the intermediate region solutions (3.17) in terms of q, and matching as $\bar{R}\to+\infty$ gives an intermediate solution in terms of Q. These two must be equivalent if we are to have a mode which simultaneously satisfies both boundary conditions, which after a little algebra gives the connection formula

$$\pi\alpha\sqrt{\frac{2}{-k_c''\epsilon}} = n\pi + \tan^{-1}\left(\frac{Q-q}{1+qQ}\right). \tag{3.19}$$

The neglected terms in (3.16) would give an $O(1)$ correction to the $O(\epsilon^{-1/2})$ phase of (3.17), and hence introduce additional $O(1)$ terms to (3.19). Therefore, retaining the leading-order term only, we find that the accumulation rate for the nearly-convected modes is:

$$\epsilon \sim \left(\frac{2\alpha^2}{-k_c''}\right)\frac{1}{n^2} \propto +\frac{1}{n^2} \tag{3.20}$$

as $n \to \infty$, where α^2 is given by (3.16) and, together with k_c'', is evaluated at $r = d$. This is a new result and is verified numerically in § 3.4. It is worth pointing out that this correct answer would not be obtained by applying the 'narrow annulus approximation' used in Golubev & Atassi (1998). Making the narrow annulus approximation (i.e. $1 - h = O(\epsilon)$) here, one would be applying the boundary conditions in the inner region, where ϕ has the form $\sin(\alpha(r-d)/\epsilon + c_2)$. This would lead to an incorrect accumulation rate with $\epsilon \propto 1/n$. In contrast, for the exponential accumulation of § 3.1 there was no such complication, and the fastest radial oscillations were directly involved in the matching procedure with the outer solution. This combination of circumstances is the reason why the 'narrow annulus approximation' gave the correct asymptotic accumulation rate for that case when applied by Golubev & Atassi (1998).

As we have argued, the scenario of this subsection should be a fairly common situation, and indeed the slow accumulation of the modes is an important point. For instance, anyone attempting a numerical investigation of an unsteady problem in swirling flow will find that many more nearly-convected modes must be accounted for in this case before an infinite sum of the contributions can be truncated. Indeed, we see that in this case, the mode shapes of the nearly-convected modes are much more oscillatory than in the previous subsection (where the phase only grew logarithmically as $\epsilon \to 0$), so it appears that any numerical computations will be notably more difficult in this case. Having argued from figure 2 that the situation leading to (3.20) is generic, we note that the rigid-body swirl with uniform axial flow considered by both Golubev & Atassi (1998) and Heaton & Peake (2005) is genuinely a special case, for which the the 'inner region' spans the entire duct $h \leqslant r \leqslant 1$. The accumulation rate, $\epsilon \propto n^{-1}$, found by both those previous investigations is therefore correspondingly different from that derived in this subsection. We emphasize that, in general, the asymptotic accumulation rate of any neutrally propagating nearly-convected modes is one of (3.8) or (3.20), depending on whether the maximum/minimum of $k_c(r)$ occurs at a wall radius or at an internal duct radius, respectively.

Finally in this subsection, we note that when (3.12) fails, the solution for real ϵ must be non-oscillatory in the inner region, and mode accumulation is not possible. Mode accumulation can occur when (3.12) fails, but then we need complex ϵ, and this is discussed in the next subsection.

3.3. *Infinite accumulation of unstable nearly-convected modes*

We return to the case of the previous subsection, assuming a situation as depicted in figure 2 and considering modes with wavenumber given by (3.10), and ask what happens when (3.12) fails. We will find that clustering can still occur, only now with a complex value of ϵ. The modes occur in complex conjugate pairs and since all nearly-convected modes propagate downstream (for full details see the discussion immediately after (4.7)), those with negative imaginary parts are convective instability modes.

We now amend the arguments of § 3.2 as required. When (3.12) fails, we will show in the next section that the flow is always algebraically unstable. In addition, the flow may possess an accumulation of unstable modes, and we consider that phenomenon here by taking ϵ complex, so that

$$k = k_c(d) + \epsilon \equiv k_c(d) + \xi + \mathrm{i}\eta \quad (\xi, \eta \in \mathbb{R}), \tag{3.21}$$

with $|\epsilon| \ll 1$. Since any modes occur in conjugate pairs we restrict ourselves to $\eta < 0$ without loss of generality.

$$\text{For } r < d: \begin{cases} f_1(r) & \text{s.t.} \quad f_1(r) \sim (r-d)^{-1}\exp(\Theta) \\ f_2(r) & \text{s.t.} \quad f_2(r) \sim (r-d)^{-1}\exp(-\Theta) \end{cases} \quad \text{as } r \nearrow d.$$

$$\text{For } r > d: \begin{cases} g_1(r) & \text{s.t.} \quad g_1(r) \sim (r-d)^{-1}\exp(\Theta) \\ g_2(r) & \text{s.t.} \quad g_2(r) \sim (r-d)^{-1}\exp(-\Theta) \end{cases} \quad \text{as } r \searrow d.$$

TABLE 2. The outer region solutions for § 3.3. Away from $r = d$ they are smooth and $O(1)$, but only calculable numerically. The quantity Θ is defined by (3.13).

Drawing on the experience of the previous subsection, we anticipate that large and real Frobenius exponents, with the RSPs again located off the real line in the complex r-plane, will be responsible for oscillatory behaviour and nearly-convected modes. This will indeed be the case, and we can quickly construct an argument similar to before. The extra complication of the present case is that the solution of the governing equation with complex k is complex. In the real problems above it was sufficient to deduce that the behaviour of the outer solution had sensitive oscillatory dependence on ϵ to conclude that the boundary conditions would be satisfied by varying ϵ. In contrast, a complex solution cannot necessarily be adjusted to satisfy the boundary conditions as both real and imaginary parts must be zero simultaneously.

The outer region, $r - d = O(1)$, has an essential singularity as before with Λ having a double zero at $r = d$. The behaviour of the outer solutions close to the essential singularity is, however, different, as can be seen in table 2.

To proceed, we look in detail at the intermediate region, the coordinate $\bar{R}$ being given by (3.14). The leading-order equation is again of WKB type,

$$\frac{\mathrm{d}^2\Upsilon}{\mathrm{d}\bar{R}^2} = \frac{|\epsilon|}{(\epsilon - |\epsilon|k_c''\bar{R}^2/2)^2}\left[\frac{-2Wk_c(k_c(Wr)' - mU')}{r^2U^2}\right]\Upsilon + O(\epsilon^{-1/2}), \tag{3.22}$$

where we define $\Upsilon \equiv (1 - |\epsilon|R^2k_c''/2\epsilon)\phi$ and all quantities U, W and k_c are evaluated at $r = d$. On setting ϵ real and positive, (3.22) reduces to (3.15), the analogous intermediate region equation of the previous subsection. Note that by assumption, the term in square brackets in (3.22) is real and positive, and labelling this now as α^2 (which agrees with the definition (3.16)) we have

$$\frac{\mathrm{d}^2\Upsilon}{\mathrm{d}\bar{R}^2} = \frac{|\epsilon|\alpha^2\Upsilon}{(\epsilon - |\epsilon|k_c''\bar{R}^2/2)^2}. \tag{3.23}$$

Equation (3.23) can be solved analytically to give the two linearly independent solutions

$$\phi = \left(1 - \frac{|\epsilon|k_c''\bar{R}^2}{2\epsilon}\right)^{-1/2}\exp\left\{\pm\mathrm{i}\sqrt{1 + \frac{2\alpha^2}{k_c''\epsilon}}\tan^{-1}\left(\mathrm{i}\bar{R}\sqrt{\frac{k_c''|\epsilon|}{2\epsilon}}\right)\right\}. \tag{3.24}$$

We now wish to match (3.24) with the outer region solutions defined in table 2 as we did in the previous subsection. As before, we can see by inspection that the solutions have the correct functional form to match, and it is simply a matter of comparing the coefficients of the different solutions. This presents a technical difficulty, however, because as $r \to d$ (through real values) in the outer region, and also as $\bar{R} \to \pm\infty$ in the intermediate region, we find that one solution is exponentially larger than the other. This is overcome by suitably deforming the integration contour off the real line and into the complex r-plane. If we approach $r = d$ in the outer asymptotic region with $\arg(r - d) = \pm\mathrm{i}\pi/2$ then the two solutions to be matched are both of

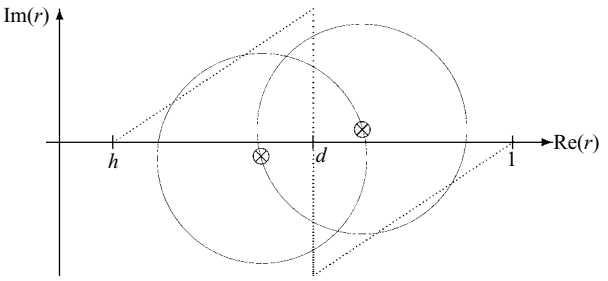

FIGURE 4. A schematic picture of the regular singular points (i.e. the critical layers), shown by $\otimes$, when $k_c''(d) < 0$ and $\eta < 0$. When $\xi < 0$, $|\eta| \ll |\xi| \ll 1$ the RSPs are very close to the real line. Also shown are the circles of convergence of each Frobenius solution and (by the dotted line) the deformed integration contour.

the same order and can be matched simultaneously. Deforming the contour is a thought experiment which allows us to correctly carry out the matching, but it is also a practical procedure often carried out in numerical computations. Numerically, it allows us to track terms which would otherwise become exponentially small, and has been a helpful methodology in many numerical calculations of spectra (for example, Leibovich & Stewartson 1983; Mayer & Powell 1992). Figure 4 shows a typical layout in the complex r-plane.

Proceeding to match now, along a deformed contour, we may simply equate coefficients of the solutions (3.24) with those arising in the outer region solutions. As before, we suppose that the outer solutions satisfying the boundary conditions on the duct walls are given by (3.18), where '$r < d$' now means the portion of the deformed contour in figure 4 which has been deformed from the $r < d$ portion of the real axis into the upper half-plane, and similarly for '$r > d$'. The constants q, Q are again $O(1)$ and could, in principle, be determined numerically. Matching with intermediate solutions using the deformed contour gives the connection formula

$$2\pi \mathrm{i}\alpha \sqrt{\frac{2}{k_c''\epsilon}} = 2n\pi \mathrm{i} + \log \frac{q}{Q}, \tag{3.25}$$

and this now determines ϵ, and hence the wavenumber of the nearly-convected mode. Neglected terms in (3.23) would give further $O(1)$ terms in (3.25). Therefore, retaining the leading-order term only, we find that at leading order ϵ is real and $O(n^{-2})$. The imaginary part of ϵ is determined at next order by the complicated $O(1)$ terms in (3.25) and so we have $\mathrm{Im}(\epsilon) = O(n^{-3})$. We therefore conclude that

$$\epsilon = \xi + \mathrm{i}\eta, \quad \xi \sim \left(\frac{2\alpha^2}{k_c''}\right)\frac{1}{n^2} \propto -\frac{1}{n^2}, \quad \eta \propto -\frac{1}{n^3}, \tag{3.26}$$

as $n \to \infty$. The leading-order real part of ϵ ensures that a real solution in the outer region $r < d$ eventually matches, via the intermediate region solutions, onto a real solution in $r > d$ (and vice versa), allowing the boundary conditions to be satisfied.

The asymptotic scaling for ϵ (3.26) leads to a distinctive layout for the positions of the regular singular points in the complex r-plane, as is shown in figure 4. The two singularities are located very close to the real line in comparison to their total displacement from d, in contrast with figure 3 in the § 3.2 case. Although no highly oscillatory inner region is immediately obvious in (3.24), two are present: they are

centred not on $r = d$, but on the real radii of closest approach to the RSPs indicated by $\otimes$ in figure 4. These radii are given by $\bar{R} = \pm\sqrt{-2/k_c''(d)}$, at which (3.23) reduces to

$$\frac{\mathrm{d}^2\Upsilon}{\mathrm{d}\bar{R}^2} = \left(\frac{\xi\alpha^2}{\eta^2}\right)\Upsilon, \tag{3.27}$$

where we use the fact that $|\eta| \ll |\xi| \ll 1$. Hence, we do indeed find very oscillatory inner regions, in this case of width $O(\epsilon^{3/2})$, and so narrower than in § 3.2. This behaviour is hidden in (3.24) in the delicate asymptotics of $\tan^{-1}$ when its argument is close to $\pm\mathrm{i}$. In contrast, the radial behaviour is exponential rather than sinusoidal in most of the intermediate region, and this leads to mode shapes that are distinctively peaked at the two inner region radii. This phenomenon has been observed numerically, see figure 10. As $n \to \infty$ and $\epsilon \to 0$, the two peaks become closer together and more pronounced.

We note for completeness the results of reworking our arguments in the case that $k_c(r)$ has a minimum value at an internal duct radius, $h < d < 1$. All the arguments follow as before, the only difference being that the change in sign of $k_c''(d)$ implies a change in sign for ξ in (3.26) above. This ensures, as before, that ϵ is real to leading order and the real parts of the Frobenius exponents are $O(\epsilon^{-1/2})$ large. The appropriate signs are easy to remember by noting that in both cases the results give the modes lying just above or below the continuous spectrum C_k in the complex plane (see figure 8).

The infinite family of unstable modes described in this subsection (and their complex conjugates) are in fact the finite wavenumber versions of the modes first discussed by Leibovich & Stewartson (1983) and later termed *ring modes*. Leibovich & Stewartson (1983), and subsequent follow-up papers, used large-wavenumber ($|m| \gg 1$) asymptotics and WKB theory to predict the existence of unstable modes at large $|m|$ for swirling flows. We have generalized those results to finite wavenumber by describing the accumulation of infinitely many instability modes. The details of the correspondence between the modes described here and those of Leibovich & Stewartson (1983) are discussed more fully in § 6.

3.4. *Numerical demonstration of clustering*

We conclude this classification of the clustering of nearly-convected modes with some numerical results. We first give a case for which the predicted accumulation is of the exponential type and the modes are neutrally propagating. The result (3.8) was first given by Golubev & Atassi (1998), but they do not present a full numerical validation. We take, for an example, the axial and swirl velocities

$$U(r) = \tfrac{1}{2} + \tfrac{1}{10}r^4, \quad W(r) = \tfrac{1}{2}r^4. \tag{3.28}$$

The duct is taken to be $h \leqslant r \leqslant 1$ with $h = 0.5$, the temporal frequency $\omega = 10$ and the azimuthal wavenumber is $m = 3$. In this case, $k_c(r)$ is monotonic for $0.5 \leqslant r \leqslant 1$ and the theory of § 3.1 predicts exponential accumulation of modes, given by (3.8), on both ends of the branch cut C_k. Choosing to label the nearly-convected modal wavenumbers k_n, where the $n = 1$ mode is the farthest from the cut, then plots of $\log(k_n - k_c(0.5))$ and $\log(k_c(1) - k_n)$ versus n should be straight lines (for n large enough) with gradients of $-\pi/\mathrm{Im}(\sigma(0.5))$ and $-\pi/\mathrm{Im}(\sigma(1))$, respectively. We find the eigenvalues numerically by integrating (2.21), decomposed as in (2.22–2.23), and using a standard variable step size integrator. Figure 5*a* shows these plots for the accumulation at both ends of the cut. The symbols are from the numerically determined modal wavenumbers,

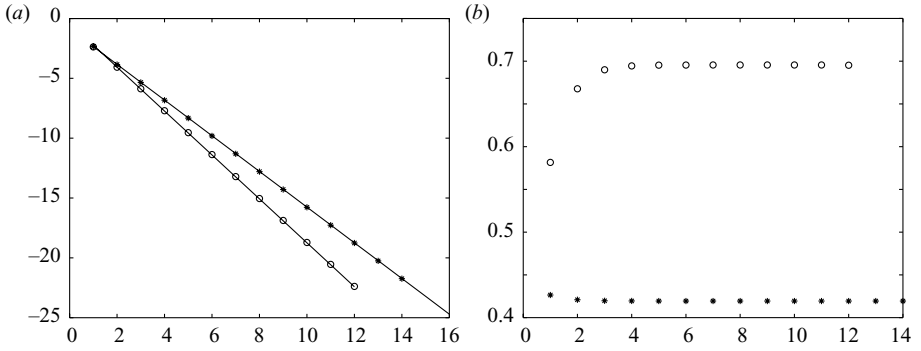

FIGURE 5. (*a*) $\log(k_n - k_c(h))$ and $\log(k_c(1) - k_n)$ against n. ○, nearly-convected modes near $k_c(h)$; *, nearly-convected modes near $k_c(1)$. The numerically found modal wavenumbers are compared to the solid lines, which are drawn at the predicted gradient. (*b*) $(k_n - k_c(h))\exp(\pi n/\mathrm{Im}(\sigma(h)))$ and $(k_n - k_c(1))\exp(\pi n/\mathrm{Im}(\sigma(1)))$ against n.

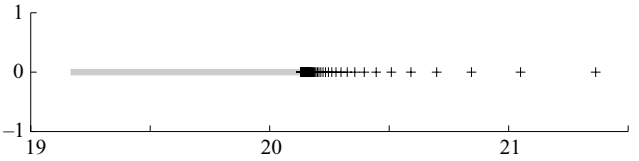

FIGURE 6. The complex k-plane in the case (3.28) with $m = -3$, i.e. stable algebraically accumulating nearly-convected modes. The continuous spectrum C_k is shown by a thick grey line, and the stable nearly-convected modes by + signs.

and the lines are drawn at the predicted gradient. The excellent agreement of the two confirms that the modes are accumulating at the predicted rate. Figure 5*b* shows the wavenumbers with the predicted exponential factor cancelled out, and we see that in both cases this quantity approaches a constant value as (3.8) would predict.

Merely changing the sign of the azimuthal order, so that $m = -3$ and the disturbances are counter-rotating instead of co-rotating, then the same parameters give a problem for which § 3.2 is required. We now expect algebraic accumulation of neutrally propagating nearly-convected modes. The maximum value of k_c is $k_c(d) = 20.13$, occurring at $r = d = 0.5588$, and (3.12) holds so that clustering of modes with $0 < k - 20.13 \ll 1$ occurs at the slower algebraic rate given by (3.20). Figure 6 shows the location of the calculated modes relative to the continuous spectrum in the complex k-plane. Figure 7*a* shows $\log(k_n - k_c(d))$ against $\log n$ plotted for the first 1500 nearly-convected modes. The convergence to the asymptotic rate is extremely slow, and very many modes must be found to be well into the asymptotic regime, which implies very highly oscillatory solutions. Nevertheless, the gradient of figure 7*a* is indeed approaching the predicted value of -2 as figure 7*b* demonstrates. This contrasts strongly with the exponential accumulation shown in figure 5, where the accumulation is quicker and hence the modes are closer to the end of the continuous spectrum C_k, and better approximated by the asymptotic regime, for much smaller values of n. In addition, the coefficient of the algebraic decay given in (3.20) agrees with the numerical results with relative error $< 2\,\%$.

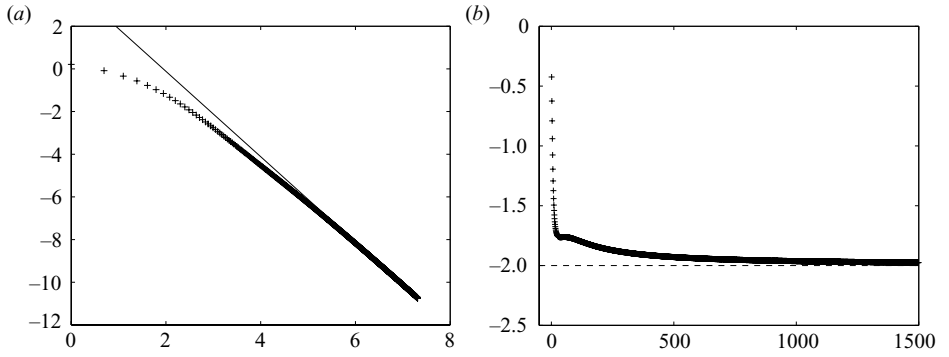

FIGURE 7. (*a*) $\log(k_n - k_c(d))$ against $\log n$. Each + represents a nearly-convected mode, the straight line is drawn with gradient -2, as predicted by the large n asymptotics. (*b*) the gradient of the former log–log plot is shown against n, and is seen to approach the predicted value of -2 for large n.

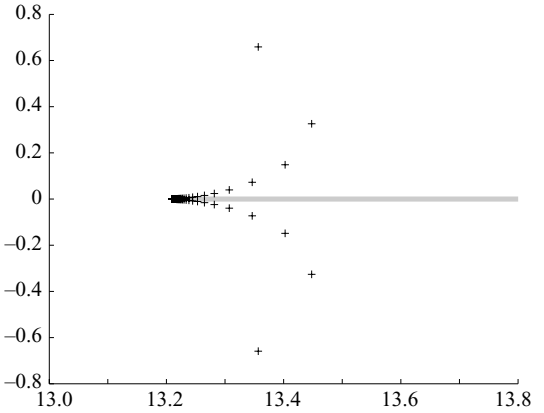

FIGURE 8. The complex k-plane near the lower end of the continuous spectrum, which is shown by a thick grey line. The nearly-convected modes are shown by + signs.

Finally, we present an example of the clustering of complex eigenvalues described in § 3.3. We take the axial and swirl velocities

$$U(r) = 0.7 - 0.5r^2, \quad W(r) = 0.1r + 0.25/r, \tag{3.29}$$

and the inner duct radius is again $h = 0.5$. The temporal frequency is $\omega = 3$ and the azimuthal wavenumber is $m = -5$. The continuous spectrum C_k in this case is found to be the set of wavenumbers $13.21 \leqslant k \leqslant 23.75$, where the maximum value $23.75 = k_c(1)$ but the minimum value $13.21 = k_c(0.6596)$ is achieved at an internal radius of the duct. The modified Rayleigh condition (3.12) fails at $r = d = 0.6596$ and so accumulation of the type (3.26) is observed (note that the classical Rayleigh stability criterion, $W(Wr)' > 0$, is satisfied everywhere by this flow). Note that here modes are clustering at the lower end of the continuous spectrum, so that $\xi \propto +1/n^2$, as explained in the paragraph following (3.26). Figure 8 shows the locations of the first 106 unstable modes in the complex plane and their complex conjugates, which are stable modes. The modes accumulate just above and below C_k as predicted. Figure 9*a* shows log–log plots for the real and imaginary parts of the modal wavenumbers against $\log n$. The curves for the real and imaginary parts both approach

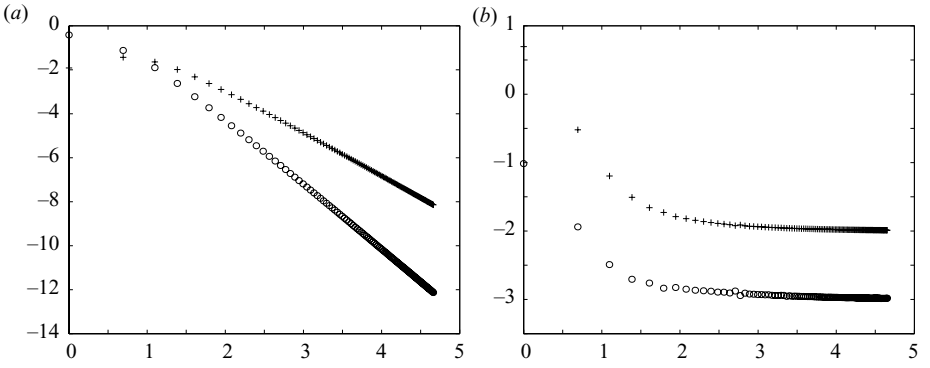

FIGURE 9. For the accumulating unstable nearly-convected modes (a) +, $\log(\mathrm{Re}(k_n - k_c(d)))$; ○, $\log(|\mathrm{Im}(k_n)|)$, versus $\log n$. (b) The gradients of the former lines, plotted with the same corresponding symbols.

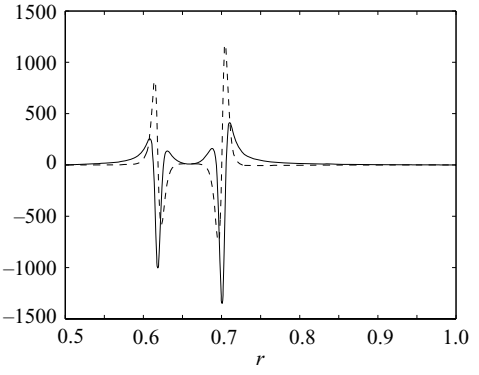

FIGURE 10. The real (solid line) and imaginary (dashed line) parts of the mode shape ϕ versus r for the $n = 5$ unstable nearly-convected mode. In this case, the radius $d = 0.6596$.

a straight line for large n, and figure 9b verifies that they are of the predicted gradients, i.e. -2 and -3, respectively. The coefficient for the $1/n^2$ decay of $\mathrm{Re}(k_n - k_c(d))$ given by (3.26) is found to agree with that of the numerical results with relative error $<1\,\%$. An example of the mode shape of these unstable modes is shown in figure 10. The mode is very strongly peaked at the two radii on either side of $r = d = 0.6596$ which correspond to the closest approach to the RSPs, as depicted in figure 4. As $n \to \infty$ and $\epsilon \to 0$, these two peaks approach $r = d$ and also become more pronounced. For larger n, we also see more oscillations of the mode shape in the inner regions at the two peaks.

4. The Green's function in swirling flow

We now discuss the behaviour of unsteady disturbances considering all the various components of the whole spectrum, including the cut C_k. The present paper is the first investigation into the contribution of the continuous spectrum (or 'convected modes') to the unsteady fields in a swirling flow, and for definiteness we choose here to work out the Green's function for the linear unsteady disturbances as our prototype problem. Of course, the solution to many problems can be constructed by appropriately convolving the Green's function with forcing quantities, so this enables us to investigate the generic properties of the flow.

The Green's function we consider is the response to a small localized mass source embedded in the flow. After decomposing as a Fourier series in θ we therefore add, without loss of generality, forcing to the right-hand side of the continuity equation (2.6) of the type

$$f = \delta(x - x_0)\delta(r - r_0)\delta(t - t_0)\mathrm{e}^{\mathrm{i}m\theta}. \tag{4.1}$$

Note that using this Fourier series representation for the θ dependence (4.1) corresponds to a ring source in the flow, and this is all we need consider to construct general forcing. In any given problem, the forcing will determine an amplitude for this Green's function, which will give after integrations and summation over m the full unsteady fields. Causality is enforced by the condition $\phi_G \equiv 0$ for $t < 0$. We take Fourier transforms in x and t and we concentrate on a single temporal frequency ω so we only need invert the spatial Fourier transform. Causality considerations for this single-frequency response will define the inversion contour for the spatial Fourier transform, by a standard application of the Briggs–Bers procedure. After factoring out the dependence on θ and dropping the explicit dependence on ω for ease of notation, we solve for the remaining complex amplitude $\tilde{\phi}_G(k, r)$ of the Green's function. The forced version of the mode-shape equation (2.21) is now

$$\frac{1}{r\rho_0}\frac{\mathrm{d}}{\mathrm{d}r}\left(\frac{r\rho_0\Lambda(G\tilde{\phi}_G + \Lambda\tilde{\phi}'_G)}{D}\right) - \frac{G}{D}(G\tilde{\phi}_G + \Lambda\tilde{\phi}'_G) + \tilde{\phi}_G\left(\frac{\Lambda^2}{c_0^2} - \frac{m^2}{r^2} - k^2\right) = \exp(-\mathrm{i}kx_0 + \mathrm{i}\omega t_0)\delta(r - r_0), \tag{4.2}$$

subject to the same boundary conditions (2.24) on the duct walls, and with the conditions that $\tilde{\phi}_G$ is continuous at the forcing radius $r = r_0$, but with a jump in derivative given by

$$[\tilde{\phi}'_G]^{r=r_0+}_{r=r_0-} = \exp(-\mathrm{i}kx_0 + \mathrm{i}\omega t_0)\left(\frac{D}{\Lambda^2}\right)_{(k,r_0)}. \tag{4.3}$$

In (4.3) and herein we group functions in round brackets with a single argument to simplify notation where necessary (for instance we write $(DG)_{(k,r)}$ for $D(k, r)G(k, r)$).

We define two solutions of the homogeneous version of equation (4.2) to be $u_1(k, r)$ and $u_2(k, r)$ which satisfy the boundary conditions that $(Gu + \Lambda\partial u/\partial r) = 0$ at $r = h, 1$, respectively, and $r\rho_0 u = 1$ at $r = h, 1$, respectively. In terms of these functions we can now write down the solution for the Green's function $\tilde{\phi}_G$ which satisfies all the boundary conditions and the jump condition (4.3) as

$$\tilde{\phi}_G(k, r) = \left(\frac{D}{\Lambda^2(u_1u'_2 - u_2u'_1)}\right)_{(k,r_0)} \exp(-\mathrm{i}kx_0 + \mathrm{i}\omega t_0)\begin{cases} u_2(r_0, k)u_1(r, k), & r < r_0, \\ u_1(r_0, k)u_2(r, k), & r > r_0. \end{cases} \tag{4.4}$$

The Wronskian in the denominator of (4.4), which is essentially the Wiener–Hopf kernel for the scattering problems described in Heaton & Peake (2005), can be simplified somewhat using the general theory of differential equations (see Bender & Orszag 1978) to give

$$\tilde{\phi}_G(k, r) = \frac{\exp(-\mathrm{i}kx_0 + \mathrm{i}\omega t_0)r_0\rho_0(r_0)}{f(k)}\begin{cases} u_2(r_0, k)u_1(r, k), & r < r_0, \\ u_1(r_0, k)u_2(r, k), & r > r_0, \end{cases} \tag{4.5}$$

where the function $f(k)$ is given by

$$f(k) = \left(\frac{\Lambda}{D}\right)_{(k,h)}(\Lambda u'_2 + Gu_2)_{(k,h)}. \tag{4.6}$$

Note that $f(k)$ is zero precisely when k is an eigenvalue wavenumber.

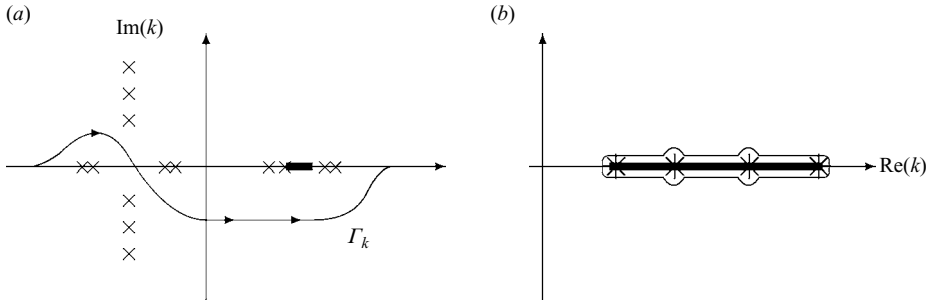

FIGURE 11. Schematics of the typical Fourier inversion contour (*a*) due to the Briggs–Bers procedure to ensure causality and (*b*) after closing in the upper half-plane and encircling C_k. In (*b*) $k_c(r)$ is monotonic and the singularities within C_k are at $k_c(r)$ and $k_c(r_0)$, plus the ends of the cut, $k_c(h)$ and $k_c(1)$.

Recall that we have explicitly cut the complex k-plane along C_k so that, for $k \notin C_k$, $\Lambda(k, r) \neq 0$ for $h \leqslant r \leqslant 1$. Hence for $k \notin C_k$, all the quantities in (4.5–4.6) are well defined and calculable. The only other singularities of $\tilde{\phi}_G(k, r)$ are the values of k such that $f(k) = 0$. These are isolated and simply correspond to modal wavenumbers. We invert the axial Fourier transform to find the Green's function by taking

$$\phi_G(x, r) = \frac{1}{2\pi} \int_{\Gamma_k} \tilde{\phi}_G(k, r) \mathrm{e}^{\mathrm{i}kx} \, \mathrm{d}k, \tag{4.7}$$

where the integration contour Γ_k is shown in figure 11*a*. The integration contour Γ_k in (4.7) is determined by causality considerations and is found by the following Briggs–Bers procedure. As $\mathrm{Im}(\omega) \to +\infty$, all the singularities of the integrand (i.e. C_k and poles corresponding to modal wavenumbers) lie away from the real k-axis and the inversion contour is the real k-axis, $-\infty < k < +\infty$. Then $\mathrm{Im}(\omega)$ is reduced to zero through positive values and analytic continuation is preserved by deforming the integration contour in the k-plane when singularities of the integrand move onto the real k-axis. Acoustic modes can originate from either $\mathrm{Im}(k) > 0$ or $\mathrm{Im}(k) < 0$ in this procedure, and hence can be right or left travelling, respectively. If we assume that $U(r) > 0$ in the duct, then (2.25) and (2.10) imply that C_k lies in the upper half-plane whenever $\mathrm{Im}(\omega) > 0$. Any nearly-convected modes as described in § 3 also originate from $\mathrm{Im}(k) > 0$ when $\mathrm{Im}(\omega)$ is large and positive: in all cases, these modes rely for their existence on an RSP being located close to the interval $[h, 1]$ in the complex r-plane, and so they must always lie near C_k in the k-plane. Hence the continuous spectrum and the nearly convected modes must lie above Γ_k, as shown in figure 11*a*, and contribute to the integral downstream of the forcing, when $x > x_0$ and the contour is closed in the upper half-plane. The convected contributions generally propagate in the direction of the flow, and at the local speed of the flow.

The integrand in (4.7) is an analytic function of k and r (except for the discontinuous radial derivative (4.3)) for all $k \in \Gamma_k$, and hence $\phi_G(x, r)$ is also analytic for $r \neq r_0$. When $x < x_0$ and the contour is closed in the lower half-plane, the discontinuity (4.3) which occurs at $k = k_c(r_0) \in C_k$ does not contribute and the response is analytic at $r = r_0$. In contrast for $x > x_0$, the contour is closed in the upper half-plane and in this region we see that $\partial\phi_G/\partial r$ is discontinuous at $r = r_0$. However, note that the radial velocity (the inverse transform of $\partial\tilde{\phi}_G/\partial r + \mathscr{R}$, see (2.12)) is continuous, as required by mass conservation. Similarly the pressure is continuous, but the axial and azimuthal unsteady velocities are discontinuous at $r = r_0$, $x > x_0$. This is the familiar response

to singular forcing (e.g. see Rienstra 1984 or Heaton & Peake 2005); the response to a smooth forcing is of course smooth, being an integration of the Green's function over a range of r_0.

4.1. *Downstream behaviour of the Green's function and flow stability*

We are now in a position to compute the Green's function via (4.7), so we turn to a discussion of the nature of $\phi_G(x, r)$. The pole contributions to (4.7) simply give modal behaviour in the Green's function. The mode is neutral if k is real. If k is complex and has not crossed the real k-axis during the Brigs–Bers procedure the mode is evanescent, if it has crossed the axis, as in the case of the modes of figure 8 below the real axis, the mode is unstable and exponentially growing and the flow is convectively unstable. The sum of contributions from the infinity of cut–off sonic modes (see figure 1) converges, and can be truncated for evaluation as for acoustic modes in irrotational compressible flow. The discrete nearly-convected modes are all propagating at close to the local flow speed, and there may be an infinity of these pole contributions to add together. A demonstration that this sum indeed converges sufficiently well is an important point, but we omit the details here as sufficient description has been made of the nearly-convected modes in §§ 3.1–3.3 to make the calculation fairly straightforward. We merely state the results, which are that in all cases the residue contribution to the Green's function ϕ_G decays like

$$Res\big(\tilde{\phi}_G(k, r)\big)_{k=k_n} = O\left(\frac{\mathrm{d}\epsilon}{\mathrm{d}n}\right) \tag{4.8}$$

as $n \to \infty$, where ϵ is the difference between the eigenvalue wavenumber of a nearly-convected mode and the end of the cut C_k, as defined in (3.2), (3.10) or (3.21). Therefore the contributions of the nearly-convected modes sum like either $\sum \mathrm{e}^{-n}$ or $\sum 1/n^3$ as $n \to \infty$, depending on which of (3.8), (3.20) or (3.26) is the appropriate accumulation rate. For a detailed discussion of the convergence of similar sums, albeit in a somewhat special case (rigid-body swirl and uniform axial flow), see Heaton & Peake (2005).

The discrete modes accounted for, we now collapse the contour Γ_k onto C_k and determine the nature of the convected contribution. Behaviour is determined by the nature of any singularities of $\tilde{\phi}_G(k, r)$ for $k \in C_k$, and the resulting behaviour of ϕ_G is typically of algebraic rather than exponential type. As a first case to consider, we assume that $k_c(r)$ is monotonic (i.e. the case of § 3.1) and for definiteness increasing, so that, if they exist, the nearly-convected modes accumulate exponentially. The integration contour is depicted in figure 11(*b*). All of $f(k)$, $u_1(k, r)$ and $u_2(k, r)$ in (4.5) can be calculated for values of k just above and below C_k by suitable continuation: for example, if k is just above the cut then the corresponding RSP of (2.21) is just above the real axis in the r-plane (because we have assumed $k_c' > 0$). Hence the correct limit as $\mathrm{Im}(k) \to 0+$ is that the RSP moves onto the real interval $[h, 1]$ and the integration contour for the quantities f, u_1 and u_2 deforms below the RSP in the r-plane, if necessary, to avoid the singularity. In the case of $f(k)$, we have to integrate all the way from $r = 1$ to h, so deformation of the contour off the real axis is always necessary, making (the analytic continuation of) $f(k)$ complex valued for $k \in C_k$. This means that $f(k)$ will not, in general, pass through zero on C_k and so there will be no complications of propagating modes embedded in the continuous spectrum. In other situations more complicated deformations in the r-plane may be required, but are easy to construct. For instance if, at the limiting value of $k \in C_k$, there are two critical layers at which k_c' has different signs (as in the case of figure 2

if $k_c(1) < k < k_c(d)$), then the contour will be deformed above one RSP, cross back through the real r-axis and pass under the second RSP.

Thus, by deforming integration contours in the complex r-plane if required, the limit of the integrand $\tilde{\phi}_G$ is well defined and calculable as k approaches a value on the cut from above or below, at most points of C_k. Singularities in $\tilde{\phi}_G(k, r)$ for $k \in C_k$ occur when this deformation procedure breaks down and no analytic continuation is possible. In the case at hand, where $k_c(r)$ is monotonic and there is only one critical layer for every wavenumber on the cut, the values of k on the cut at which $\tilde{\phi}_G$ is singular are just $k = k_c(h)$ and $k_c(1)$, the ends of the cut, and $k = k_c(r)$ and $k_c(r_0)$. This is because these values of k correspond to the singularity $\Lambda = 0$ occurring at the end points in the integration of (4.2). For instance, when calculating $u_1(r_0, k)$ we integrate the homogeneous version of (4.2) from $r = h$, with the conditions on $r = h$ given before (4.4), to the point $r = r_0$. If $k = k_c(r_0)$ or $k = k_c(h)$, i.e. the RSP is one of the end points of the integration, it is not possible to deform the r integration contour away into the complex plane, since the contour is pinned at $r = r_0$ and $r = h$, respectively. Similarly, when calculating $u_2(r, k)$ we find singularities when $k = k_c(r), k_c(1)$ owing to the r integration contour being pinned at r and 1. Since we cannot analytically continue $\tilde{\phi}_G(k, r)$ to these wavenumbers, the integration contour in the k-plane should be indented to avoid them, as depicted in figure 11(b). A portion of the inversion integral along any line segment just above or below the cut which does not include one of these indentations is $O(1/x)$ as $x \to \infty$ (far downstream of the forcing location), by a simple application of the Riemann–Lebesgue lemma to (4.7). The leading behaviour of the continuous spectrum part of the Green's function for large x is thus governed by the contributions from the neighbourhoods of the singular values on the cut C_k.

Now, consider an inversion of the type (4.7) with $\tilde{\phi}_G$ smooth, except that in the neighbourhood of some 'singularity' $\hat{k}$ it has algebraic behaviour of the type

$$\tilde{\phi}_G \sim (k - \hat{k})^s, \tag{4.9}$$

where $\mathrm{Re}(s) \leqslant -1$ and a suitable branch is chosen. One can show, again by straightforward contour deformation and application of the Riemann–Lebesgue lemma, that the large-x behaviour of the inversion integral for a contour that approaches, indents around, and then departs away from the singularity is of the form

$$\phi_G \sim \mathrm{e}^{\mathrm{i}\hat{k}x} x^{-s-1} \left(\frac{2\pi \mathrm{i}^s}{\Gamma(-s)} + o(1) \right). \tag{4.10}$$

If $\mathrm{Re}(s) > -1$, then the contribution is all $o(1)$, i.e. tends to zero as $x \to \infty$. This result allows for a classification of the large-x behaviour of the Green's function for inviscid swirling pipe flow in terms of the strength of the singularities of its transform $\tilde{\phi}_G$ on the cut C_k. With $\sigma(r)$ given by (2.28), the singularity in $\tilde{\phi}_G$ at $k = k_c(r)$ and $k = k_c(r_0)$ is algebraic like (4.9), with exponents $s = \sigma(r), \sigma(r_0)$, respectively. The nature of the singularities at the ends of the cut $k = k_c(h), k_c(1)$ requires a little more thought, but using the critical-layer analysis of § 2, we find that the exponent is zero. The ends of the cut are in fact not singular at all and the wall radii are not special, because in (4.5) the singularities in $u_{1,2}$ at $k = k_c(h), k_c(1)$ are exactly cancelled by singularities in $f(k)$. Clearly, the form that the exponents $\sigma(r)$ take in this problem varies greatly as the mean flow properties are varied in (2.28), leading to many different possible cases. Consider the singularity at $k_c(r)$. The most striking case is when $A(r) < 0$, then one of the exponents at the critical layer has $\mathrm{Re}(\sigma) < -1$,

in which case the large-x asymptotics, i.e. (4.10) with $s = \sigma$, imply that the convected continuous spectrum grows algebraically without bound in the downstream direction. Similarly the contribution from the neighbourhood of $k = k_c(r_0)$ grows if $A(r_0) < 0$, with both singularities contributing to ϕ_G. This algebraic instability is a new result, and is much stronger than that which has been found in two-dimensional mean flow, see for example Landahl (1980). This is one of the main results of the current paper.

In the simplest case, for which $k_c(r)$ is monotonic, $k_c(r)$ and $k_c(r_0)$ are the only two singularities on C_k for a given r and r_0. Note that in this case any nearly-convected modes present are of the type described in § 3.1, and are hence neutrally stable. If $A(r) < 0$, then the Green's function $\phi_G(x, r)$ grows algebraically for large x at radius r owing to the singularity at $k_c(r)$. If $A(r_0) < 0$, then we see that $\phi_G(x, r)$ must be growing algebraically downstream for all values of r, i.e. throughout the whole duct, because the contribution from $k_c(r_0)$ is growing. If the observation radius is the same as the forcing radius, $r = r_0$, then the two singularities combine and the exponent is doubled, because both u_1 and u_2 in (4.5) are singular at $k = k_c(r_0)$, each with exponent $\sigma(r_0)$. Hence, $\phi_G(x, r_0)$ would be growing much faster than the disturbance at nearby radii $r \neq r_0$. In any case, if an algebraic instability occurs, some radius will possess the greatest rate of algebraic growth and far downstream the response will be the growing convected disturbance, sharply peaked at this radius and dominating all modal contributions and all other radii. Note that the exponent of algebraic growth for the unsteady velocity components and unsteady pressure can differ slightly from that for the potential ϕ, as can be found from (2.8), (2.12)–(2.14). The results of the manipulations are that

$$(p', u_r', u_\theta', u_x') \sim (x^{-1}, x^{-1}, 1, 1)\phi, \tag{4.11}$$

so that the axial and azimuthal velocity grow faster than the pressure and radial velocity.

If instead $A(r) > 0$, then the effect of the neighbourhood of $k = k_c(r)$ on the downstream convected disturbance is not growing. If $A(r) > 0$ throughout $h \leqslant r \leqslant 1$, then the convected contribution is decaying for large x for all radii except for $r = r_0$, when the two singularities coincide on the cut to give an exponent with real part -1 and a contribution which neither grows nor decays downstream. This is the case in which the continuous spectrum has least effect on the Green's function far downstream.

We will provide specific numerical demonstration of the behaviour described in this section in § 4.3.

4.2. *Acute algebraic instability*

We now describe the application of the above theory to the cases of § 3.3, which have an infinite number of unstable modes. The analysis is the same as in § 4.1, with some more complicated results. A simple extension is that if there exists a radius $r_1 \neq r_0$ distinct from the forcing radius with $k_c(r_1) = k_c(r_0)$, then the two singularities associated with $k = k_c(r), k_c(r_0)$ combine when $r = r_1$. This leads to the surprising conclusion that forcing at a given radius r_0 can lead to convected disturbances far downstream which are peaked at two radii. The convected response to the forcing grows more strongly (compared to neighbouring radii) on $r = r_0$ and also at another preferred radius given by r_1.

The more important question to address, however, is what happens for r close to d (the local maximum of $k_c(r)$, see figure 2). The modified Rayleigh condition (3.12) fails in § 3.3, and hence the continuous spectrum is algebraically unstable at

radii close to d. The exponents $\sigma(r)$ are easily shown to be real, and to blow up as $\sigma(r) \sim a|r-d|^{-1}$ as $r \to d$, for some constant a (recall that the denominator in (2.29) vanishes when $k_c' = 0$). The continuous spectrum contribution, calculated just as described in the previous subsection, is 'acutely' algebraically unstable, that is with a growth exponent which blows up as $\sigma(r) \sim a|r-d|^{-1}$ as $r \to d$. The continuous spectrum, often neglected in practice, therefore exhibits asymptotic growth faster than any power of x in the neighbourhood of $r = d$. This is a somewhat alarming conclusion, and to understand the Green's function further we must also consider the unstable nearly-convected modes which are present in these cases (see § 3.3 and figure 8). In any event far downstream the most unstable mode should dominate, and singularity in our asymptotic expansion simply means we must rework our analysis a little more carefully.

Consider alone the infinite sum of nearly-convected modes: the modes are strongly peaked as shown in figure 10, the two peaks approaching $r = d$ from either side and also growing larger as the modenumber $n \to \infty$. If $r \neq d$, for sufficiently large n (small ϵ) r lies in the outer asymptotic region (see figure 4). Hence the numerators in (4.5) are finite, and since the residue of the denominator decays as $O(n^{-3})$, by (4.8), the sum converges. This argument fails when $r = d$ because, of course, $r = d$ is never in the outer asymptotic region as $n \to \infty$. Indeed, the peaks in the mode shapes which grow and converge upon $r = d$ mean that the numerators in (4.5) grow exponentially rather than tending to finite limits and hence the sum does not converge.

The important practical question is what is the Green's function response at finite values of $x > x_0$. The total Green's function is of course finite and continuous, because the integrand in (4.7) is continuous in r and on the original contour Γ_k shown in figure 11(a) the integral converges for all r. For $r \neq d$, the simplest idea works: we may subtract away the modal contributions (a convergent sum) and then treat the continuous spectrum in isolation. When $r = d$, however, one of the indentations of the contour shown in figure 11(b) is at $k_c(d)$, an end of C_k, and cannot avoid the poles of the nearly-convected modes which cluster near the end of C_k (recall figure 8). The separation of the continuous spectrum from the modes can no longer apply for $r = d$, and this resolves the apparent difficulty. The singularity which develops in the continuous spectrum contribution exactly cancels the non-convergent tail of the infinite modal sum when $r = d$.

Since it is the attempt to separate the unsteady field into modal and non-modal parts which fails when $r \simeq d$, this implies that computation of the Green's function is complicated. We will not present detailed numerical results for the modal and continuous spectrum contributions to an acutely unstable case as we have seen that such a decomposition is neither uniformly possible nor natural. Our numerical investigation of this case is limited to the results of figures 8–10 and the following comments.

(a) The infinite sum of residues from nearly-convected modes was observed to converge more slowly, and its value to grow without bound, as $r \to d$.

(b) It was possible for a limited range of $O(1)$ values of x to compute (4.7) directly via a contour encircling all the modes and C_k together. Integrating along this contour, like Γ_k in figure 11(a), means we do not attempt to split C_k from the modes. It was found that the radius d is not visibly special, in that $|\phi_G|$ is not peaked there for small x. Hence we conclude that the growth of the modal sum is smoothly cancelled by growth in the continuous spectrum contribution as $r \to d$.

We conclude that the continuous spectrum and the higher-order modes, while complicated, are each important to the near-field Greens' function and should not be

neglected without care. Although the two types of contribution are mathematically different and must be treated differently in the analysis, it is neither desirable nor wise to attempt to separate the modal and non-modal fields in a practical computation. For larger values of x, of course, the field is dominated by the most unstable mode, and the continuous spectrum can be neglected.

We note that a similar type of behaviour was observed by Heaton & Peake (2005), for the case of uniform axial flow and rigid-body mean flow, which is a special case in which the continuous spectrum collapses to a single point and the asymptotics of the nearly-convected modes are much simpler. In that case, it was seen that a conditionally convergent sum of nearly-convected modes was discontinuous at a certain radius, but that the (very degenerate) continuous spectrum adjusted to cancel this discontinuity. The major difference, however, is that Heaton & Peake (2005) considered the unsteady field scattered from a sharp edge, located at $r = s$, and it was at this radius at which the modal contribution was discontinuous. Here there is no geometrical selection of the radius $r = d$ at which the modal sum is singular, rather it is a radius chosen by the mean flow and the disturbance parameters m and ω.

In conclusion, we see that the modified Rayleigh condition (3.12) is intimately related to the stability of the flow. When (3.12) fails, $A < 0$ and the convected disturbances grow: the continuous spectrum makes the flow at least algebraically unstable, and the instability may even be exponential if $k_c(r)$ is not monotonic. Unsurprisingly, all these instabilities associated with C_k are of convective type, for which the time harmonic response at a single frequency ω grows as $x \to \infty$, and the region of growth in response to an impulsive localized forcing propagates downstream with the flow.

4.3. *Numerical calculations of the Green's function*

We present in this subsection some illustrative calculations of the Green's function described above. Our aim is to use numerical computations to verify our arguments about the nature of the response, particularly about the downstream asymptotics. A particular aim is to compare directly the contributions of the three possible portions of the spectrum of acoustic–vorticity waves, namely the acoustic and nearly-convected modes, and the continuous spectrum. No comparison of this kind has been made before, and indeed in the acoustics literature the convected and nearly-convected parts have sometimes been discarded as negligible, whereas we have seen that they can be algebraically and exponentially growing.

In the first instance, we consider a case for which the theory predicts an algebraic instability. We take the axial and swirl velocities

$$U(r) = 1 - 0.5r^2, \quad W(r) = 0.1r + 0.25/r. \tag{4.12}$$

The duct is taken to be $0.7 \leqslant r \leqslant 1$, the temporal frequency $\omega = 3.2$ and the azimuthal wavenumber is $m = -2$. For this set of parameters, $A < 0$ throughout the duct, so that the flow should be algebraically unstable. The continuous spectrum C_k in this case is found to be the set of wavenumbers $5.85 \leqslant k \leqslant 7.80$ and $k_c(r)$ is monotonically increasing. We expect no accumulation of nearly-convected modes (using § 3.1), and algebraic growth of the type described in § 4.1. In figure 12, the algebraic growth exponent predicted by the analysis of § 4 is plotted as a function of radius, and we see that in this example growth is strongest near the hub radius. Numerically, we find two propagating acoustic modes, two infinite sets of exponentially decaying cutoff acoustic modes and, as expected, no nearly-convected modes of any kind. At this frequency and azimuthal order, the spectrum has no instability modes, and the only

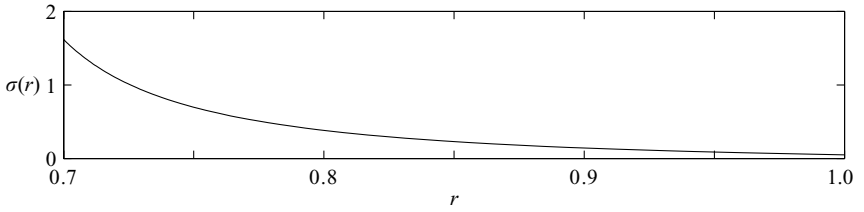

FIGURE 12. The algebraic growth exponent as a function of radius for the flow (4.12).

growth is due to C_k, which is expected to be algebraically unstable. Our interest is in the contribution of the continuous spectrum and for clarity the results presented do not include the acoustic modes. Note that this flow satisfies the standard Rayleigh criterion, which strictly only ensures stability to axisymmetric disturbances in the absence of axial shear.

The maximum algebraic growth rate in this case, as shown by figure 12, is $\sigma(0.7) = 1.62$. While this is significantly stronger than linear growth, the algebraic growth in swirling flow can of course be much stronger; however, we found that very strong algebraic growth rates are usually accompanied by instability modes being present in the spectrum as well. In our current choice of flow we have avoided cases where instability modes are present as our aim is to investigate the continuous spectrum and, although a consideration of the continuous spectrum in isolation would be mathematically correct for cases with an instability mode, it would be misleading to show very strong algebraic growth when the dominant growth is really exponential. The case shown in figure 12 was chosen for reasons of clarity for our demonstration of continuous spectrum growth, but in more complicated cases the growth can be very much stronger. We also note here a further result of our numerical investigations: on choosing parameters such that an acute instability (as described in § 4.2, for which $\sigma(r)$ is unbounded and there is an infinite chain of unstable modes) is nearly present, there are usually a finite number of unstable nearly-convected modes. For instance, if the radius $r = d$ of § 3.3 is located just outside of the duct $h \leqslant r \leqslant 1$, then the infinite tail of unstable nearly-convected modes cannot be present, but a small finite number of the unstable modes persist. As the parameters are changed to move away (in parameter space) from the acute instability, the last instability modes disappear, one by one moving towards and then disappearing into the branch cut C_k.

We calculate $\tilde{\phi}_G(k, r)$ by numerical solution of the ordinary differential equation (4.2) using a standard variable step size integrator. We invert the axial Fourier transform using adaptive Simpson quadrature for the integration, adjusting the error tolerances to verify convergence. The procedure is a challenging computation as, in order to observe the asymptotic growth, large values of x must be considered. Large values of x require $0 < -\mathrm{Im}(k) \ll 1$ on the portion of the integral beneath C_k in the k-plane, so that the exponential factor in the Fourier inversion $\mathrm{e}^{\mathrm{i}kx}$ is not too large, as this would inhibit accurate numerical evaluation of the inversion integral. Consequently, we must compute $\tilde{\phi}_G(k, r)$ close to the singular values of $k \in C_k$ and this is expensive, because it means integrating (4.2) close to the critical layer. In order to achieve this we first verified that the expected singular behaviour, of the type (4.9) with $s = -\sigma(r) - 1, -\sigma(r_0) - 1$, was present at $k = k_c(r), k_c(r_0)$, respectively. Considering the integration below C_k (the integration above C_k is treated similarly, and together they form a contour as shown in figure 11*b*), we approximate the integrand as follows. We make use of our knowledge of the Frobenius series to form a Laurent series type

approximation to the integrand close to each singular wavenumber; on cancelling the known singular factors we can numerically approximate what remains, which yields numerical values for the coefficients a_n in (2.26). The series are truncated after a few terms and we discard the second (less singular) Frobenius series in the simplest approximation. This procedure yields a numerical approximation to $\tilde{\phi}_G(k, r)$ which possesses the correct singularity structure at $k = k_c(r)$ and $k_c(r_0)$, and which therefore preserves the correct mathematical behaviour while also being cheap to calculate. For $O(1)$ values of x, it is possible to perform the numerical integration by direct computation around a rectangular contour including C_k. Good agreement was found with the Laurent series approximation described above. Since our Laurent series type approximation was verified in the near field, and by construction preserves the correct asymptotic far field, we conclude that the approximation is accurate. Because the downstream behaviour is entirely dictated by the strength of the singularities at $k = k_c(r), k_c(r_0)$, we stress that checking the singularities were actually present and of the strength predicted by the theory, before numerically removing them, is an important step.

We present some results, for which we take $x_0 = 0$ and $r_0 = 0.9$, to fix a position for the forcing. The critical-layer exponents are $\sigma(r_0) = -1.14, 0.14$ at the forcing radius, and we observe the response at $r = 0.71$, where the critical-layer exponents are $\sigma(r) = -2.32, 1.32$. The expected algebraic singularities were observed in $\tilde{\phi}_G$ at $k = k_c(r_0)$ and $k_c(r)$, and in the large-x asymptotics the singularity from $k = k_c(r)$ dominates to predict an algebraically growing response downstream with

$$\phi_G(x, 0.9) \sim \mathrm{e}^{\mathrm{i}\times 5.87x} x^{1.32} \tag{4.13}$$

as $x \to \infty$, where $5.87 = k_c(0.71)$. We performed the computations described above, and after sampling $\tilde{\phi}_G(k, r)$ for $k \in C_k$ and cancelling out the singular factors at $k = k_c(r_0), k_c(r)$ we found a pronounced, but non-singular, peak at a third wavenumber, say $k = k_{qm} \in C_k$. This peak was found to be the influence of a very close 'mode' lying on the other Riemann sheet of the complex plane, i.e. the sheet onto which the instability modes move as they disappear from the physical sheet 'into the branch cut' in the process described above. Although the mode is no longer present, its effect is still felt via a large peak in the amplitude of $\tilde{\phi}_G(k, r)$ at $k = k_{qm} \in C_k$. This effect is similar to the 'quasi-modes' discussed by Shrira & Sazanov (2001), but is not of direct importance here since its effect is dominated by the contributions from the singularities on C_k. We simply mention that the quasi-mode phenomenon was observed numerically, and that therefore knowing the functional form of the peak appearing in $\tilde{\phi}_G(k, r)$ on C_k facilitated our numerical method. This phenomenon should be very general and will occur for any parameter values, such as the current ones, which are close to an acute singularity.

Presenting now the results of the computations, figure 13 shows the continuous spectrum response in the near-field of the forcing. We see that the response 'beats' due to the interference of the range of wavenumbers present in the signal, i.e. the range of C_k on the real k-axis. A simple analysis of the signal shown in figure 13 via FFT shows that, already for these modest values of x, the signal is dominated by two wavenumbers, namely $k_c(r)$ and $k_c(r_0)$. Modulo this beating phenomenon, the strength of the response is seen to be growing in the downstream direction immediately. Figure 14(a) shows the results from the computations in the far field on a log–log plot of $|\phi_G(x, r)|$ and x. That the curve approaches a straight line for large x indicates algebraic growth. Figure 14(b) shows the gradient of figure 14(a) and we see that the predicted algebraic growth rate is obtained, verifying (4.13) and giving

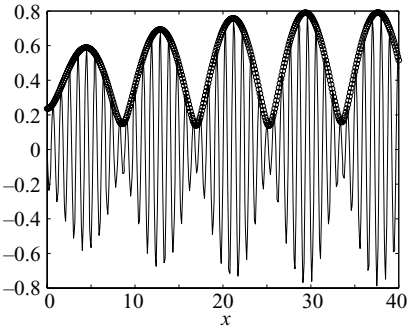

FIGURE 13. The real part (solid line) and magnitude (○ symbols) of $\phi_G(x, 0.9)$ in the near field.

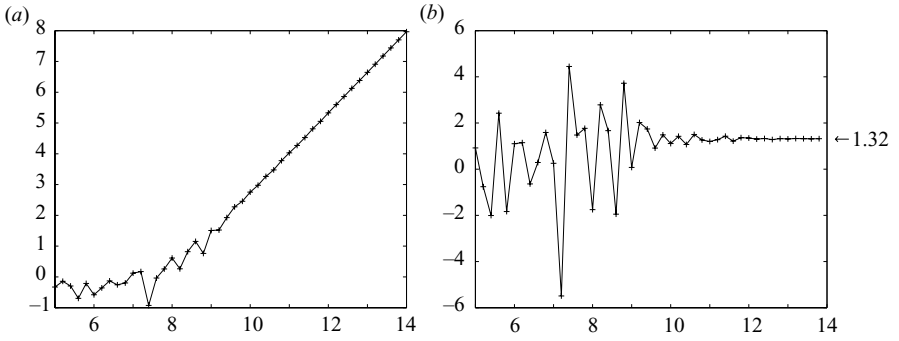

FIGURE 14. (*a*) A plot of $\log|\phi_G(x, r = 0.9)|$ against $\log x$, each + denotes a calculated value. (*b*) The gradient of the former curve is plotted and is seen to approach the predicted exponent of algebraic growth for large x.

excellent agreement with the theory. It can also be verified that far downstream the response has the phase $ik_c(r)x$.

For a second example, we return to the case used in figure 5, i.e. (3.28) with $m = +3$. For this flow with these parameters the Green's function does not possess an instability, either modal or algebraic. The spectrum has cut-on acoustic modes, two sets of nearly-convected modes (which cluster exponentially) and a continuous spectrum C_k. We choose a forcing location to be $x_0 = 0$, $r_0 = 0.7$, and now we choose to look at all the propagating contributions to the unsteady field at $x = 0+$, just downstream of the forcing. Figure 15 shows the unsteady pressure field (we choose this physical variable instead of the potential ϕ_G to make the comparison potentially more interesting) broken down into three contributions:

(*a*) the two cut-on downstream propagating sonic modes of the system (the contributions of the cutoff sonic modes are not plotted as these will be exponentially decaying in x);

(*b*) the two sets of nearly-convected modes of the system;

(*c*) the contribution from the continuous spectrum C_k.

This is the first such calculation to include the swirling flow convected spectrum, and although there is no physical problem behind these calculations as yet, it is worth briefly comparing the contributions. One would expect the pressure to be much greater from the sonic modes than anything else, and that is what we see. The continuous spectrum convected disturbance is strongly peaked at the forcing

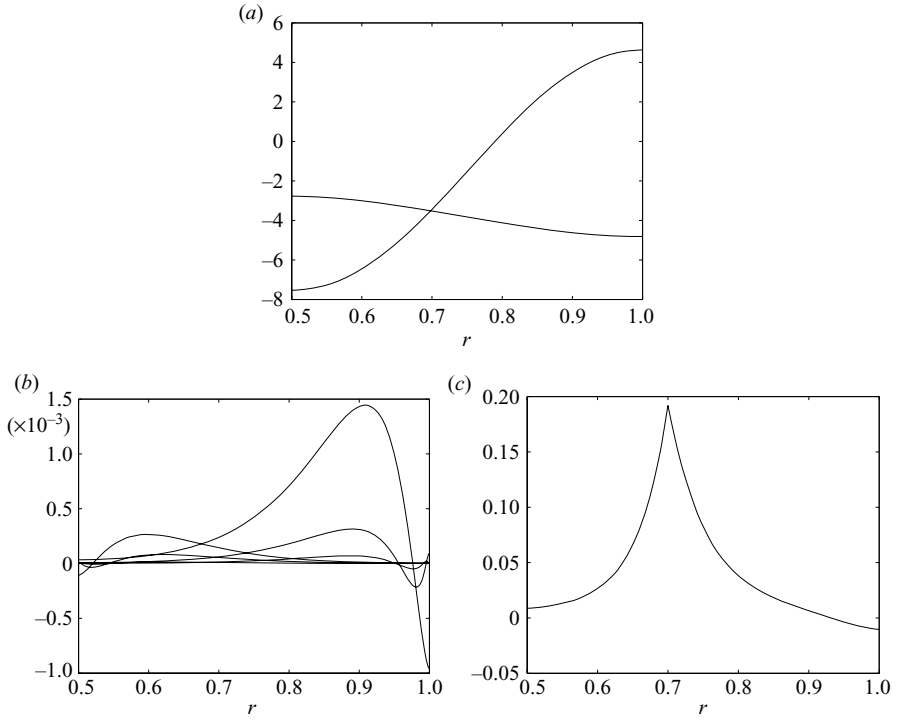

FIGURE 15. The three non-evanescent contributions to the unsteady pressure against r at $x = 0+$ from (a) the two cut-on acoustic modes, (b) the nearly-convected modes, (c) the continuous spectrum C_k.

radius and intermediate in magnitude between the modal sonic and nearly-convected pressures. Note that the pressure from the continuous spectrum in figure 15(c) is continuous, but with discontinuous radial derivative at $r = r_0$ as a consequence of (4.3). It is smooth at all other radii. The effect of C_k appears to be small for this δ-function forcing, which excites all axial wavelengths equally; however, it was seen in the scattering problems studied by Heaton & Peake (2005) that in some physical problems (e.g. scattering at a trailing edge) the response can preferentially select wavenumbers in the neighbourhood of convection. Indeed, it was seen that the nearly-convected modes can play a very important role in some configurations, so we infer from figure 15 that the continuous spectrum will be at least equally important, even ignoring the possibility of algebraic instability.

4.4. *Calculations of the unsteady vorticity*

In addition to the calculations presented above, we now give some further results obtained during investigation of the phenomenon of algebraic growth. We revert to the mean flow and parameters given in (4.12) as used in the calculations of figures 12, 13 and 14. Recall that for these parameters, the only instability is the algebraic growth of the continuous spectrum, and so with no instability modes to complicate the results this is an ideal case for investigating the algebraic growth in isolation. The results presented so far in figures 13 and 14 are for the potential ϕ_G of the Green's function solution; however, we now wish to identify the physical mechanism at play, and so instead we choose to calculate the unsteady *perturbation vorticity*, $\boldsymbol{\xi}'$. The analogous result to (4.11), for the exponent of the algebraic growth of $\boldsymbol{\xi}'$ compared

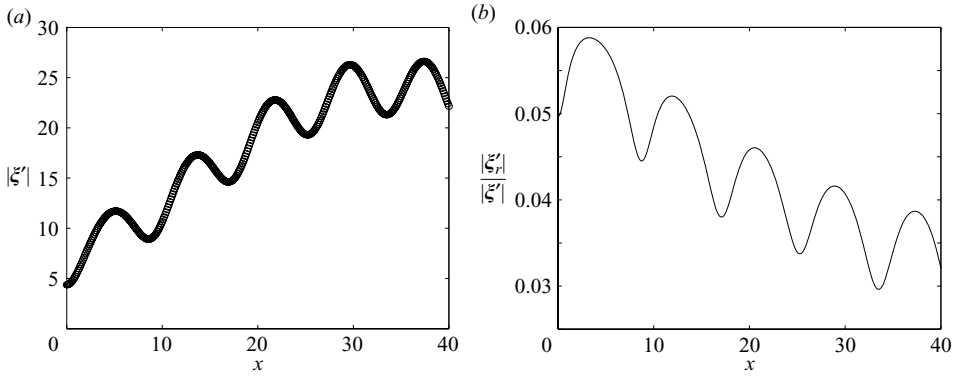

FIGURE 16. Plots of the direction and magnitude of the unsteady vorticity for $0 \leqslant x \leqslant 40$ at $r = 0.71$ (*a*) $|\boldsymbol{\xi}'|$ against x. (*b*) $|\xi_r'|/|\boldsymbol{\xi}'|$.

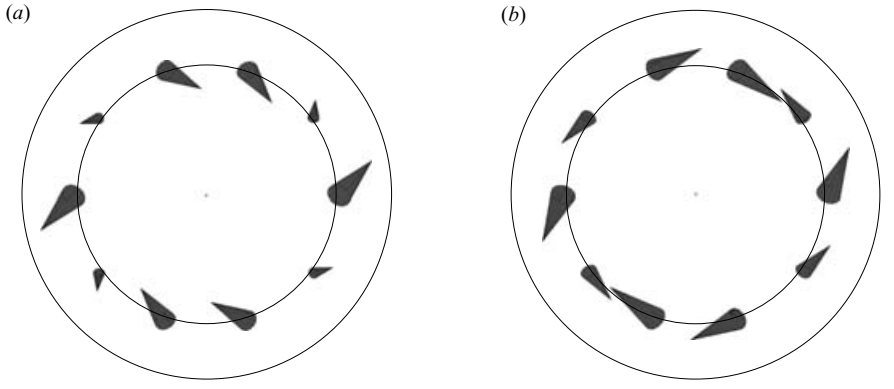

FIGURE 17. End-on views of the duct at (*a*) $x = 0$ and (*b*) $x = 150$. The duct inner and outer walls are shown at $r = 0.7, 1$ respectively, and the unsteady vorticity field at $r = 0.71$ is shown by the conical arrowheads. Note that the amplitude of $|\boldsymbol{\xi}'|$ has been scaled down by a factor of about 40 between (*a*) and (*b*) to allow comparison.

to that of ϕ, is that

$$(\xi_r', \xi_\theta', \xi_x') \sim (1, x, x)\phi \quad \text{as} \quad x \to \infty, \tag{4.14}$$

so that the unsteady vorticity grows faster in magnitude than ϕ, though not in all three of its components. We omit the majority of the details of the algebraic manipulations in this subsection, such as those leading to (4.14), as they are fairly complicated (though elementary) deductions from (2.12)–(2.14).

Figure 16 shows some numerical results for the unsteady vorticity. In figure 16(*a*) we show the magnitude of $\boldsymbol{\xi}'$, and in figure 16(*b*) we indicate its direction, at the same radius $r = 0.71$ as used in figures 12, 13 and 14. Notice that $|\boldsymbol{\xi}'|$ grows substantially, and also exhibits the same 'beating' phenomenon seen in figure 13 owing to interference of the various wavenumbers in the continuous spectrum. As for the direction of the vortex lines, they become increasingly aligned according to (4.14), i.e. lying in a surface $r = \text{const}$. Figure 17 shows end-on views of the duct at two values of x. The cones are drawn with their axes aligned in the local direction of $\boldsymbol{\xi}'$, and one can see clearly that the vortex lines become aligned with $r = \text{const}$ as we look further downstream.

The candidate mechanism for the instability is of course vortex stretching: the mean flow and perturbations we consider are fully three-dimensional and so this would explain immediately why the results for swirling pipe flow are so different from those of two-dimensional channel flow. To this end we note a result which is visible in the results of figures 16 and 17, that from (4.14) with $x \gg 1$ the unsteady vorticity to leading order has no radial component, and is dominated by its azimuthal and axial components. This behaviour is consistent with growth due to vortex stretching as there is no mean flow in the radial direction and so stretching would tend to cause growth in the θ, x components. Specifically, for constant r, the phase lines are given by

$$k_c(r)x + m\theta = \text{const}, \tag{4.15}$$

which defines a set of helices. The rate of strain of the mean flow will stretch such a helical phase line apart from a neighbouring phase line at slightly larger or smaller radius. This stretching, which occurs in the axial and azimuthal directions owing to the swirling mean flow we consider here, is the analogue of the longitudinal stretching and the resultant streaks described by Landahl (1975, 1980).

Pursuing this further, we identify the most singular terms in $\tilde{\boldsymbol{\xi}}'(k, r)$ at $k = k_c(r)$, which will therefore give the coefficient of the most strongly growing power of x far downstream. We find that

$$\tilde{\boldsymbol{\xi}}'(k, r) = \frac{\mathrm{i}r}{(Wr)'}(\boldsymbol{\xi}_0 \cdot \boldsymbol{k})\left\{\boldsymbol{\xi}_0 \frac{k_c(r)\phi}{\Lambda} - \boldsymbol{e}_\theta \phi'\right\} + O(\phi) \quad \text{as } k \to k_c(r), \tag{4.16}$$

where $\boldsymbol{\xi}_0 = (0, -U', r^{-1}(Wr)')$ is the mean flow vorticity, $\boldsymbol{k} = (-, m/r, k_c(r))$ is the phase vector of the disturbance and prime denotes differentiation with respect to r as before. The factor of $1/\Lambda$ and the prime on ϕ, respectively, cause the k singularity of the two terms in the braces in (4.16) to be stronger than that of ϕ by one power. As such the large x asymptotics of $\boldsymbol{\xi}'$ are

$$\boldsymbol{\xi}'(x, r) = (\boldsymbol{\xi}_0 \cdot \boldsymbol{k})\{\boldsymbol{\xi}_0 A(r) + \boldsymbol{e}_\theta B(r)\} x^{\sigma(r)+1} \mathrm{e}^{\mathrm{i}k_c(r)x} + O\left(x^{\sigma(r)}\right) \tag{4.17}$$

for some functions $A(r)$, $B(r)$. The most important feature of (4.17) is the appearance of the factor $\boldsymbol{\xi}_0 \cdot \boldsymbol{k}$ multiplying the leading-order response, a factor which corresponds to the operator $\boldsymbol{\xi}_0 \cdot \nabla$ acting on the unsteady flow. This confirms that vortex stretching by the three-dimensional mean flow is at the heart of the instability, since the $\boldsymbol{\xi}_0 \cdot \nabla$ operator in the vorticity equation is responsible for vortex stretching when acting on the fluid velocity. If the factor $\boldsymbol{\xi}_0 \cdot \boldsymbol{k} = 0$, then (4.17) shows that the growth rate is reduced and growth is inhibited, which corresponds to the result of Landahl (1980): namely that perturbations to a two-dimensional shear flow can grow linearly if there is a non-zero spanwise wavenumber, i.e. $\boldsymbol{\xi}_0 \cdot \boldsymbol{k} \neq 0$, and that there is no algebraic growth otherwise.

We conclude that vortex stretching is important to the algebraic instability. A more precise statement linking it to Rayleigh's inertial instability is made in § 6.

5. High-frequency asymptotics

Before placing the stability results of the present paper into context with respect to the existing literature, we give here a further new result to which they are closely related. Cooper & Peake (2005) considered linear perturbations to compressible, ducted, swirling, Euler flow, and assumed asymptotic high-frequency and large azimuthal mode number, a regime of particular practical importance in aeroacoustics

(specifically, $\omega = O(m)$ with $m \gg 1$). In the equations derived by Cooper & Peake (2005), the continuous spectrum is modelled at leading asymptotic order by a disturbance which possesses the rapid convected phase, i.e. $\propto \exp(\mathrm{i}k_c(r)x)$, and with a slowly distorting amplitude for the vortical components of velocity and the potential, $\boldsymbol{a}_0(x, r) = (a_r, a_\theta, a_x, \phi)$. The amplitudes obey an equation of the form

$$\frac{\partial \boldsymbol{a}_0}{\partial x} = \boldsymbol{M}(x, r)\boldsymbol{a}_0, \tag{5.1}$$

which is given as equation (20) of Cooper & Peake (2005). The solution of this equation is augmented by an unsteady hydrodynamic boundary layer at each of the duct walls. An analytical solution to the system of equations (5.1) for the downstream evolution of the gust amplitude has been found by M. E. Goldstein (personal communication, 2005) and is given in Appendix B of Heaton & Peake (2005). First, we make the transformation

$$Y = ma_\theta/r + k_c(r)a_x, \tag{5.2}$$

which defines a new dependent variable from which all components of $\boldsymbol{a}_0$ can be recovered (see Heaton & Peake 2005 for details). Then, letting

$$y = \mathrm{i}xk_c' \left(\frac{m^2}{r^2} + k_c^2\right)^{-1/2} \tag{5.3}$$

define a new independent variable, it can be shown after some algebraic manipulations that $Y(y, r)$ satisfies

$$(1 - y^2)Y'' - 2Y' - A(r)Y = F(r), \tag{5.4}$$

where prime denotes differentiation with respect to y, $A(r)$ is given by (2.29) and $F(r)$ is a given function of radius determined by initial conditions specified at $x = 0$ (say). Equation (5.4) is Legendre's equation and has general solution

$$Y(y, r) = -\frac{F(r)}{A(r)} + \alpha(r)P^0_{\sigma(r)}(y) + \beta(r)Q^0_{\sigma(r)}(y), \tag{5.5}$$

where P^0_σ, Q^0_σ are Legendre functions of the first and second kind, respectively. In (5.5), $\sigma(r)$ is the critical-layer exponent given by (2.28), and $\alpha(r)$ and $\beta(r)$ are simply arbitrary functions of radius to be determined by imposition of initial conditions at $x = 0$ say. In the light of the algebraic growth described in § 4, the obvious question to ask is how does this solution behave in the limit $x \to \infty$. Appealing to the general theory of Legendre functions, and in particular to equations 8.1.2, 8.1.3 and 8.2.2 of Abramowitz & Stegun (1964), we find that

$$Y(y, r) \sim y^{max(\sigma(r), -\sigma(r)-1)} \tag{5.6}$$

as $|y| \to \infty$. In other words, this solution grows algebraically for large x if

$$max(\sigma(r), -\sigma(r) - 1) > 0, \tag{5.7}$$

which is precisely when $A(r) < 0$, i.e. when the modified Rayleigh condition (3.12) fails. Hence, the solutions of the leading-order high-frequency equations exactly reproduce the algebraic growth of the continuous spectrum described in § 4. The algebraic growth rates for each physical quantity, which as given by (4.11) vary slightly from that of ϕ, can each be shown to be the same for solution (5.5) as those derived from the analysis of § 4. Indeed, the high-frequency asymptotic solution exhibits exactly the correct growth exponents, so it even has singular behaviour corresponding to the

'acute' algebraic growth described in § 4.2. As the radius d, at which $\sigma(d) = \infty$, is approached the large-x asymptotic growth rate of the solution (5.5) blows up.

While the high-frequency asymptotics are seen to represent accurately the continuous spectrum, the nearly-convected modes are not captured by the scalings of Cooper & Peake (2005). To include this effect, one should use the analysis presented in § 3.

6. Relations to previous work on swirling flow stability

This section aims to put the stability results of the previous sections into the context of previous work on the stability of swirling flows. First we discuss the continuous spectrum, and from the analysis of § 4 we recall that algebraic growth of the continuous spectrum occurs when

$$\frac{2Wk_c}{r^2}(k_c(Wr)' - mU') < 0, \tag{6.1}$$

with $k_c(r)$ being given by (2.10). Criterion (6.1) reduces to the famous stability criterion of Rayleigh (1916) for rotating flow (i.e. $U = 0$) to axisymmetric instabilities when either: $m = 0$ and the disturbances are indeed axisymmetric, or $U' \equiv 0$ and the axial flow is not sheared. An important point to note is that the algebraic growth of § 4 is not an effect of compressibility (c_0^2 does not appear in the growth rate or stability criterion), and that the same results hold for incompressible swirling flow as well. To be precise, equation (18) of Howard & Gupta (1962) is the incompressible version of (4.2), and it is seen to have exactly the same critical-layer structure as (4.2). Hence the corresponding incompressible problem has the same growth when $A < 0$ with the same algebraic growth rate. We therefore compare our result to previous investigations of both compressible and incompressible stability of inviscid swirling flow. Also, the precise nature of the boundary conditions (hard or soft wall) and flow geometry (hollow or annular duct, or unbounded flow) do not affect the critical-layer analysis and the algebraic instability.

That (6.1) is reminiscent of Rayleigh's criterion for rotating fluid suggests that the mechanism for this growth of the continuous spectrum is the same as the inertial instability. Just so, since (6.1) holds when the scalar product of disturbance wavenumber and mean flow vorticity (both of which are defined immediately following (4.16)) is negative for a wavenumber belonging to the continuous spectrum C_k: this restatement of the inertial instability in terms of a scalar product being given in the Appendix of Pedley (1969). The investigations of Pedley (1968, 1969) concern instabilities in swirling pipe flow not associated with the critical layer, and so are not directly relevant to the present paper. Also, the mean flows of those papers are somewhat special (they are asymptotically close to a rigid-body swirl superimposed on uniform inviscid flow, and Poiseuille viscous flow, respectively); in this section, the stability results available for general swirling (and sheared) flows are of most interest.

Many authors have previously considered the stability of swirling flows from various perspectives, and there is a large literature on the subject. Most treatments make some sort of simplifying assumption such as streamwise independent disturbances, or axisymmetric disturbances, or that the mean flow is rigidly rotating. In any case, almost all the theoretical work on stability has concentrated on the search for unstable modes, and as such the non-modal continuous spectrum growth of § 4 is complementary to those results. Some explicitly algebraic behaviour has been found by authors investigating the temporal stability of two-dimensional shear flows, see Case (1960) for an introduction and Hanifi & Henningson (1998) for a more recent

paper. Some non-integral algebraic decay rates have been noted previously also, for example Brown & Stewartson (1980) found, for stratified two-dimensional shear flows, decay exponents depending on the Richardson number. However, considering two-dimensional problems is a simplification in itself and seems to lead to less than generic behaviour. Both Ellingsen & Palm (1975) and Landahl (1980) find indications that three-dimensionality is a crucial ingredient in these problems: they observed that two-dimensional mean flows can exhibit linear growth, but only if the unsteady perturbations are themselves three-dimensional. Presumably it is for precisely this reason that the algebraic growth found in two-dimensional flows is not as strong as we have found here in a three-dimensional swirling flow: the papers mentioned found that the disturbance could increase at most linearly with time in a two-dimensional shear flow, whereas the exponent for the algebraic instability found here can take any value (depending on flow parameters via (2.28)).

That comparison can be made between the linear temporal growth with $k = 0$ found by Ellingsen & Palm (1975), or the linear spatio-temporal growth found by Landahl (1980) and the spatial growth of the present paper requires a little justification. First, we could have alternatively worked here at a fixed wavenumber k (the temporal problem), in which case we would have obtained the same growth in the time evolution of disturbances on inversion of the temporal Fourier transform by very similar manipulations. Thus the growth rates we have found in the spatial problem correspond exactly to the temporal problem. The growth rate results are still a little artificial, however, holding only for the spatial (fixed ω) or temporal (fixed k) problems. What is really important is the full space–time development of a disturbance belonging to the continuous spectrum, and we can generalize our results as follows. The space–time evolution of the response to general forcing is obtained from our results by evaluating

$$\Phi(x, r, \theta, t) = \int_{-\infty}^{\infty} \int_{\Gamma_k} \mathscr{F}_a(k, \omega) \tilde{\phi}_G(k, r, \omega)\, \mathrm{e}^{\mathrm{i}kx + \mathrm{i}m\theta - \mathrm{i}\omega t}\, \mathrm{d}k\, \mathrm{d}\omega\,, \tag{6.2}$$

for some forcing amplitude $\mathscr{F}_a(k, \omega)$. The integral over k is performed as outlined in § 4, and we assume it gives an algebraically growing result for $x \to \infty$, say

$$\int_{\Gamma_k} \mathscr{F}_a(k, \omega) \tilde{\phi}_G(k, r, \omega)\, \mathrm{e}^{\mathrm{i}kx}\, \mathrm{d}k \sim f(r, \omega) x^{\sigma} \mathrm{e}^{\mathrm{i}k_c(r)x}. \tag{6.3}$$

Then inserting this into (6.2) and considering $x = U(r)t$, $r\theta = W(r)t$, because the disturbance propagates with the local mean flow velocity, we see using Laplace's method that

$$\Phi(x, r, \theta, t) \sim \int_{\infty}^{\infty} \mathrm{d}\omega f(r, \omega) x^{\sigma} \sim g(r) \frac{x^{max_{\omega}\sigma}}{\sqrt{\log x}} \quad \text{as } t \to \infty. \tag{6.4}$$

The exponent σ contains dependence on ω, and so the full solution contains growing components at all the exponents possible from the excited frequencies. This result says that the disturbance is convected downstream, and that far downstream it grows algebraically (in x and t), being dominated by the fastest growing component available amongst the excited frequencies. The maximum growth rate $max_{\omega}\sigma$ can easily be found from (2.28). Thus, modulo a small $\sqrt{\log x}$ correction, the algebraic growth of the continuous spectrum is the same for fixed ω, the spatial problem, or fixed k, the temporal problem, as for the full space–time evolution.

We can now, in fact, recover the results of the investigators of two-dimensional shear flows from our results, the correct limit to take being that of no swirl. Letting

$W(r) \equiv 0$ in (2.28) gives $\sigma = 0, -1$, which in turn implies that the disturbance velocities can be constant as $x \to \infty$ in the spatial problem, or as $t \to \infty$ in the temporal problem. Also note that in the case of no swirl, the growth exponent $\sigma \equiv 0$ in (6.4), and no $\sqrt{\log x}$ correction appears as Laplace's method need not be applied to the integral. Therefore the unsteady velocities are constant in the large-x, t evolution for a non-swirling mean flow. As is explained by Landahl (1980), this result coupled with the linear growth of the spatial extent of the envelope, which grows as $(U_{max} - U_{min})t$ during the evolution of the initial disturbance, completes the argument: the streamwise integrated momentum of the disturbance must grow linearly with x, t, in agreement with the results of Ellingsen & Palm (1975) and Hanifi & Henningson (1998), and the disturbance kinetic energy also grows linearly with x, t in agreement with the results of Landahl (1980). The no-swirl limit of our result has recovered these results satisfactorily. With swirl, the principal difference is the form of the growth rate σ which can take much larger values, and also there is the less important introduction of the $\sqrt{\log x}$ factor in (6.4) owing to the dependence of σ on ω.

Although the algebraic growth we have identified is a new result, some criteria are available in the literature which guarantee stability of swirling flows to all types of disturbance. The strongest and most general results we have been able to find regarding the overall stability of compressible inviscid swirling flows are those of Lalas (1975). The algebraic growth due to the continuous spectrum is additional to any modal exponential instabilities that may be present in the problem, and should be consistent with the sufficient conditions for overall stability found by Lalas (1975). Equation (3.6) of Lalas (1975) is an inequality which, when satisfied, ensures the stability of a general swirling inviscid flow to disturbances of a given wavenumber k and azimuthal order m. We write that inequality here as

$$\mathscr{L}(m, k, r) \geqslant 0, \tag{6.5}$$

for $h \leqslant r \leqslant 1$. The headline sufficient condition for the stability of swirling flow to any disturbance, given in the introduction to Lalas (1975), is found by bounding $\mathscr{L}(m, k, r)$ below with an expression independent of k and m. Because our flow is homentropic and neutrally stable to gravitational/centrifugal instability (as $N^2 = 0$ where N is the effective Brunt–Väisälä frequency given by (2.20)), we can never satisfy that stability condition, but progress is still possible. After some algebraic manipulation, it is possible to show that Lalas's quantity can be written as

$$\mathscr{L}(m, k, r) = N^2 + \left(U' + \frac{m}{k}\left(\frac{w}{r}\right)'\right)^2 \left\{A(m, k, r) - \tfrac{1}{4}\right\}\left(1 + \frac{m^2}{k^2 r^2}\right)^{-1}, \tag{6.6}$$

where $A(m, k, r)$ is given by (2.29), but with $k_c(r)$ replaced by a general wavenumber k. The derivation of the sufficient condition for stability (6.5) uses a general energy-type approach, analogous to the well-known proof of Rayleigh's and Fjørtoft's theorems for parallel shear flow (see Drazin & Reid, p. 131, 1981), which means that when (6.5) fails, nothing can be said about flow stability. If we set $N = 0$, then (6.6) implies that $A(m, k, r) > 1/4$ is sufficient for stability, which is compatible with our results since the algebraic instability is present if and only if $A(m, k_c(r), r) < 0$ for some r. Our results also imply the following statement: a swirling, homentropic, inviscid flow is stable if and only if $A(m, k_c(r), r) > 0$ for all $m \in \mathbb{Z}$ and $h \leqslant r \leqslant 1$, and there are no modal instabilities. If the first condition fails, then the flow has a convective algebraic instability, if the second fails, then the flow has a modal instability, either convective or absolute. This statement may be useful as there is a large literature concerned

with the presence of modal instabilities, and anyway they can often be found by standard application of the Briggs–Bers procedure. On the other hand, the results of this paper allow an easy determination of whether any growth of the continuous spectrum occurs.

We now discuss the other new result on swirling-flow stability presented in this paper, the infinite chain of unstable modes described in § 3.3 and its associated 'acute' algebraic instability described in § 4.2. The modes are finite $|m|$ analogues of the modes originally found by Leibovich & Stewartson (1983) using WKB theory under the assumption of $|m| \gg 1$. To justify this statement we note again that $k_c'(d) = 0$ implies that the denominator of A in (2.29) vanishes at that radius. Therefore, using this to eliminate m in favour of $k_c(d)$ in the modified Rayleigh condition (3.12), we find that the cases of § 3.3 correspond to

$$W\left(\frac{W}{r}\right)'\left\{\left(\frac{W}{r}\right)'(Wr)' + U'^2\right\} < 0, \tag{6.7}$$

evaluated at $r = d$. Condition (6.7), if it holds at any point in the flow, is exactly the criterion given by Leibovich & Stewartson (1983) for modal instability for large $|m|$. The converse argument is also true: if (6.7) holds at some radius d in the flow, then there is an 'acute' algebraic instability and the opportunity for an infinity of unstable nearly-convected modes. To see this, we can choose a single frequency and observe the complex k-plane. If we take

$$\omega = -m\left(\frac{U}{U'}\left(\frac{W}{r}\right)' - \frac{W}{r}\right)_{r=d} \tag{6.8}$$

then (6.7) implies that we have an acute instability with $k_c(d)$ given by

$$k = k_c(d) = -m\frac{1}{U'}\left(\frac{W}{r}\right)'_{r=d} \quad . \tag{6.9}$$

Alternatively, we could choose a single real wavenumber according to (6.9), in which case the acute instability would be seen in the complex ω-plane at the frequency given by (6.8).

We therefore conclude that our results recover the sufficient condition (6.7) of Leibovich & Stewartson (1983) for instability in a swirling flow. We have further shown that at finite $|m|$, the modes form an infinite family accumulating towards the end of the continuous spectrum. This accumulation was described in detail in § 3.3, and a numerical example was given in figures 8 and 9. We also see that our results, as interpreted above and noting the form of (6.8)–(6.9), are valid for all values of $m \neq 0$. This is an extension of the results of Leibovich & Stewartson (1983), which were only valid for asymptotically large $|m|$. Indeed, an advantage of our results is that they provide mathematical analysis and details for general flows in $O(1)$ parameter regimes, rather than in some asymptotic regime (e.g. large $|m|$, near-neutral, etc). Our results go some way to explain the findings of various investigators: Leibovich & Stewartson (1983) themselves state that their numerical calculations appear to show many unstable modes for each m, and similar observations were made by Duck & Foster (1980) and by Duck (1986). Also, only modest values of $|m|$ (the value of $m = -4$ used by Leibovich & Stewartson (1983) is typical) are used in the numerical calculations which find the unstable modes predicted by WKB theory. A full explanation of the phenomenon is now given by the analysis of § 3 above, in which m was held fixed. We note that such an infinite chain of instability modes

is not necessary for exponential instability: as mentioned during the computations of § 4.3, if an acute instability is nearly present, e.g. if ω is just outside the range of frequencies given by (6.8), then a small finite number of unstable modes persist. On moving farther from an acute instability in parameter space, e.g. by varying ω, the remaining unstable modes one by one move toward and disappear into the branch cut (continuous spectrum) C_k. Finally, as argued from figure 4 previously and demonstrated numerically in figure 10, the unstable modes of § 3.3 are concentrated near to $r = d$ (recall they posses two narrow peaks, one either side of $r = d$). We note that these are the modes described as 'ring modes' and investigated by Stewartson & Capell (1985), again via large $|m|$ asymptotics.

To summarize, we have identified a previously unknown convective non-modal instability caused by the purely convected wavenumbers of the continuous spectrum, for which the growth is algebraic in the downstream coordinate. The exponent of this algebraic growth has been determined in terms of mean flow quantities and can take any value, indeed in many cases it is arbitrarily large close to some internal radius of the duct. Our analysis gives a necessary and sufficient condition for this growth, which is compatible with a relevant sufficient stability condition in the existing literature. In addition, modal instabilities may also be present, and when they are the results of § 3.3 considerably further the understanding of the spectrum of hydrodynamic instabilities in swirling flow. For a more complicated flow, other features will enter, for instance gravity or non-uniform entropy, and will have a stabilizing (or destabilizing) effect on the flow in the usual way, but this is not the issue of immediate interest here.

7. Summary

In this paper, we have considered various aspects of acoustic–vorticity wave perturbations to inviscid swirling flow. We have described the wavenumber spectrum with some care and classified the phenomenon of accumulation of nearly-convected eigenvalues at the edges of the continuous spectrum. To summarize: the clustering can be either exponential or algebraic, and of the three possibilities for accumulating nearly-convected modes, one was found to be a family of instability modes, for which the detailed analysis describes the modes of Leibovich & Stewartson (1983) when $|m| = O(1)$. The continuous spectrum itself was seen to be responsible for a convective instability with algebraic growth when (6.1) holds, a condition which reduces to Rayleigh's criterion if the disturbances are axisymmetric, or the axial flow profile unsheared. The algebraic instability is stronger than that found in two-dimensional shear flow and can be very strong, despite being algebraic and not exponential, because of the form of the growth exponent, given by (2.28) and (4.11). When the algebraic growth is at its very strongest and the family of unstable nearly-convected modes is also present, the separation of the modal and non-modal contributions requires care. Further work on the response in these cases is in progress.

Finally, we reflect on the aeroacoustic implications of this work. Obviously, any instabilities in the flow through an aeroengine could tend to lead to higher noise levels. A particular example of this is the tonal noise created by the convected disturbances shed from the fan being scattered by the downstream stator blades. Alternatively, convected disturbances shed from the stators might amplify as they pass along the bypass duct, before being converted into sound by edge scattering at the exit. Typically, there is a small, but non-zero, amount of swirl in the bypass duct, but on the other hand the disturbances have a relatively long distance to propagate, so that it is not beyond question that the sort of algebraic effect described in this paper could play a role. Of course, in this scenario one could seek to measure the effects we

describe relative to the (more conventional) radiation of downstream-going acoustic duct modes in the bypass, but we believe that this issue requires further attention.

REFERENCES

Abramowitz, M., & Stegun, I. A. 1964 *Handbook of Mathematical Functions*. Dover.

Bender, C. M. & Orszag, S. A. 1978 *Advanced Mathematical Methods for Scientists and Engineers*. McGraw–Hill.

Bers, A. 1983 Space–time evolution of plasma instabilities – absolute and convective. In *Handbook of Plasma Physics* (ed. M. N. Rosenbluth & R. Z. Sagdeev), vol. 1, pp. 451–517. North-Holland.

Briggs, R. J. 1964 *Electron-stream Interactions with Plasma*. MIT Press.

Brown, S. N. & Stewartson, K. 1980 On the algebraic decay of disturbances in a stratified linear shear flow. *J. Fluid Mech.* **100**, 811–816.

Case, K. M. 1960 Stability of inviscid plane Couette flow. *Phys. Fluids* **3**, 143–148.

Cooper, A. J. & Peake, N. 2005 Upstream-radiated rotor–stator interaction noise in mean swirling flow. *J. Fluid Mech.* **523**, 219–250.

Drazin, P. G. & Reid, W. H. 1981 *Hydrodynamic Stability*. Cambridge University Press.

Duck, P. W. 1986 The inviscid stability of swirling flows: large wavenumber disturbances. *Z. Angew. Math. Phys.* **37**, 340–360.

Duck, P. W. & Foster, M. R. 1980 The inviscid stability of a trailing line vortex. *Z. Angew. Math. Phys.* **31**, 524–532.

Ellingsen, T. & Palm, E. 1975 Stability of linear flow. *Phys. Fluids* **18**, 487–488.

Goldstein, M. E. 1978 Unsteady vortical and entropic distortions of potential flows round arbitrary obstacles. *J. Fluid Mech.* **89**, 433–468.

Golubev, V. V. & Atassi, H. M. 1998 Acoustic–vorticity waves in swirling flows. *J. Sound Vib.* **209**, 203–222.

Hanifi, A. & Henningson, D. S. 1998 The compressible inviscid algebraic instability for streamwise independent disturbances. *Phys. Fluids* **10**, 1784–1786.

Heaton, C. J. & Peake, N. 2005 Acoustic scattering in a duct with mean swirling flow. *J. Fluid Mech.* **540**, 189–220.

Howard, L. N. & Gupta, A. S. 1962 On the hydrodynamic and hydromagnetic stability of swirling flows. *J. Fluid Mech.* **14**, 463–476.

Lalas, D. P. 1975 The 'Richardson' criterion for compressible swirling flows. *J. Fluid Mech.* **69**, 65–72.

Landahl, M. T. 1975 Wave breakdown and turbulence. *SIAM J. Appl. Math.* **28**, 735–756.

Landahl, M. T. 1980 A note on an algebraic instability of inviscid parallel shear flows. *J. Fluid Mech.* **98**, 243–251.

Leibovich, S. & Stewartson, K. 1983 A sufficient condition for the instability of columnar vortices. *J. Fluid Mech.* **126**, 335–356.

Mayer, E. W. & Powell, K. G. 1992 Viscous and inviscid instabilities of a trailing vortex. *J. Fluid Mech.* **245**, 91–114.

Nijboer, R. 2001 Eigenvalues and eigenfunctions of ducted swirling flows. *AIAA Paper* 2001-2178.

Pedley, T. J. 1968 On the instability of rapidly rotating shear flows to non-axisymmetric disturbances. *J. Fluid Mech.* **31**, 603–607.

Pedley, T. J. 1969 On the instability of viscous flow in a rapidly rotating pipe. *J. Fluid Mech.* **35**, 97–115.

Rayleigh, Lord 1896 *The Theory of Sound*, vol. 2, § 369. Macmillan.

Rayleigh, Lord 1916 On the dynamics of revolving fluids. *Proc. R. Soc. Lond.* A **93**, 148–154.

Rienstra, S. W. 1984 Acoustic radiation from a semi-infinite duct in a uniform subsonic mean flow. *J. Sound Vib.* **94**, 267–288.

Shrira, V. I. & Sazonov, I. A. 2001 Quasi-modes in boundary-layer-type flows. Part 1. Inviscid two-dimensional spatially harmonic perturbations. *J. Fluid Mech.* **446**, 133–171.

Stewartson, K. & Capell, K. 1985 On the stability of ring modes in a trailing line vortex: the upper neutral points. *J. Fluid Mech.* **156**, 369–386.

Tam, C. K. W. & Auriault, L. 1998 The wave modes in ducted swirling flows. *J. Fluid Mech.* **371**, 1–20.